Renewable Energy 243 (2025) 122540

Contents lists available at ScienceDirect

Renewable Energy

journal homepage: www.elsevier.com/locate/renene

Power production assessment of wave energy converters in mainland Portugal

Ajab Gul Majidi [a,b,*], Victor Ramos [a,b], Paulo Rosa-Santos [a,b], Luciana das Neves [a,b,c], Francisco Taveira-Pinto [a,b]

[a] Department of Civil Engineering, Faculty of Engineering of the University of Porto (FEUP), Rua Dr. Roberto Frias, S/N, 4200-465 Porto, Portugal

[b] Interdisciplinary Centre of Marine and Environmental Research of the University of Porto (CIIMAR), Avenida General Norton de Matos, S/N, 4450-208 Matosinhos, Portugal

[c] IMDC—International Marine and Dredging Consultants, Van Immerseelstraat 66, 2018 Antwerp, Belgium

ARTICLE INFO

Keywords:
Marine energy concession zones
Offshore energy
Renewable energy
Sustainability
Wave farms

ABSTRACT

This study presents a detailed performance assessment of a wide variety of Wave Energy Converters (*WECs*) across the coast of mainland Portugal, which presents one of the largest wave energy resources in continental Europe. Furthermore, the analysis is extended to the six concession zones designated by the Portuguese government for the exploitation of offshore renewable energy. For this purpose, a 44-year historical wave data analysis obtained through a high-resolution numerical model is used to estimate key performance parameters of 18 case-study *WECs*. The results highlight the coastal area in the vicinity of Figueira da Foz (Central Portugal) as a particularly promising location for *WEC* deployment, validated by the high Annual Energy Production (above 4 GWh), capacity factor, and favorable capture width values. Conversely, the southern locations of the Portuguese shore do not appear to present favorable conditions for the *WECs* analyzed, largely due to lower wave energy availability and less optimal sea states. Additionally, this study emphasizes the need for research efforts to improve energy capture efficiency to fully utilize wave energy as a key component of the energy mix.

1. Introduction

The global commitment to combat climate change and reduce reliance on fossil fuels has catalyzed a profound transformation in the energy sector, necessitating a shift toward sustainable, environmentally responsible, and carbon-neutral energy solutions. To achieve this, it is essential to broaden and diversify the energy mix with alternative renewable sources. In this context, wave energy stands out as a promising option due to its substantial global availability, high predictability compared to other intermittent sources, and minimal environmental footprint [1–3].

However, the development of reliable and commercially viable Wave Energy Converter (*WEC*) technologies has, thus far, proven elusive, and no standard *WEC* design has yet emerged [4]. Numerous concepts based on different operating principles—such as point absorbers, attenuators, oscillating water columns, overtopping devices, and oscillatory surge converters—have been proposed, but none has gained universal acceptance as the optimal solution [5]. This slow progress can be attributed to two primary factors. First, *WECs* face substantial technical challenges due to the complexity of the conversion process, which includes energy absorption, transmission, generation, and conditioning [3]. Each of these stages often require specialized control strategies to optimize efficiency across a wide range of wave conditions. Second, the harsh marine environment, particularly in offshore areas with strong wave climates, poses substantial risks to the durability of *WECs*, escalating both operational and maintenance costs [6]. This limited technological progress has also led to gaps in essential industrial expertise, including supply chain management, logistics, and key operational aspects like deployment, maintenance, grid integration, and decommissioning. Consequently, the current Levelized Cost of Energy (*LCoE*) for wave energy remains high, estimated between 0.30 and 0.55 $/kWh, rendering it commercially unviable at present [7].

In consequence, for wave energy to become economically viable, further advancement in *WEC* technology is essential, with a focus on

* Corresponding author. Department of Civil Engineering, Faculty of Engineering of the University of Porto (FEUP), Rua Dr. Roberto Frias, S/N, 4200-465 Porto, Portugal.

E-mail addresses: ajabgulmajidi@gmail.com (A.G. Majidi), jvrc@fe.up.pt (V. Ramos), pjrsantos@fe.up.pt (P. Rosa-Santos), lpneves@fe.up.pt (L. das Neves), fpinto@fe.up.pt (F. Taveira-Pinto).

https://doi.org/10.1016/j.renene.2025.122540
Received 4 June 2024; Received in revised form 26 December 2024; Accepted 28 January 2025
Available online 31 January 2025

enhancing efficiency and reliability while reducing costs [8]. In this regard, assessing WEC performance under real-world conditions is crucial for enhancing device efficiency and durability, reducing costs, and ultimately supporting the economic feasibility of large-scale deployment [9]. To achieve this, two main approaches are available. For *WEC* technologies at high Technology Readiness Levels (TRL), physical testing of scaled devices in wave basins and/or offshore test sites (Table 1) offers crucial insights into device performance and resilience under extreme wave conditions [10]. Conversely, for *WEC* technologies at lower TRLs, evaluating performance across diverse wave conditions and locations is crucial to guide development and optimization [11]. In this early stage, numerical modeling, particularly spectral wave models, offers a cost-effective and consistent approach for such assessments [12]. Spectral wave models provide detailed characterization of coastal wave conditions over extended periods, capturing the spatial and temporal variability of the wave resource. This insight is critical for accurately evaluating WEC performance and viability in diverse marine environments. Additionally, it supports device optimizations, such as aligning the device's natural frequency with incoming waves to achieve resonant mode operation and velocity amplification, ultimately resulting in a quadratic increase in energy extraction [13].

In the context of *WEC* development, Portugal has emerged as a key player due to its substantial wave energy resource, reaching up to 35 kW per meter of wave front [34]. The central region holds the highest potential for WEC deployment at depths around 50 m, followed by the northern region and specific areas of the southern coast with favorable seabed morphology [35,36]. As a result, the interest in harnessing Portugal's wave energy resource has driven the development of testing sites and power facilities. These initiatives have become instrumental in advancing diverse *WEC* technologies and solidifying Portugal's role in the wave energy sector [35]. On these grounds, the CorPower Ocean project known as HiWave-5 stands out. The project entails the first-ever full-scale *WEC* deployment by the company off the coast of Portugal [37]. As a result, the CorPower C4 device with 9 m diameter, 18 m height, 300 kW rated power, and 70 tons weight [38], assembled in Viana do Castelo and towed offshore to the Aguçadoura test site, was connected to the national grid via a subsea cable. In addition, Eco Wave Power has achieved a significant regulatory milestone by securing approval from the Portuguese government for the installation and grid connection of a 1-MW wave energy project. The project will be deployed on the ocean side of the north breakwater of river Douro mouth, in the city of Porto [39]. These milestones align with Portugal's National Energy and Climate Plan for 2021–2030 (PNEC 2030), aiming to reach 70 MW of wave power capacity by 2030 [39]. To support this goal, six concession zones along the coast have been designated for the commercial development of offshore renewables (offshore wind and wave energy), as shown in Fig. 1. Furthermore, plans are also underway to complete the installation of an international offshore energy testing center by 2026 [40].

While the wave resource in Portugal has been adequately characterized in previous research [41,42], a comprehensive assessment of power production across a diverse array of *WEC*s with varying operational modes and principles is still lacking. Most studies to date have focused on specific *WEC* technologies and locations, often using wave hindcast data with limited temporal and spatial resolution. For example, Rusu et al. assessed the performance of four *WEC* concepts—Pelamis, Aqua Buoy, Wave Dragon, and Archimedes Wave Swing—based on a 3-year wave hindcast for selected regions along the northern and central Portuguese coast [43]. Similarly [36,44,45], examined the performance of the CECO device in various operational modes along the Portuguese coast, but the analysis was confined to water depths of 30, 40, and 50 m and based on a limited 11-year hindcast wave dataset. Ribeiro et al. evaluated the historical and near-future efficiency of two *WEC*s (Aqua Buoy and Pelamis) using a SWAN model under the RCP 8.5 climate change scenario. However, their analysis was limited to these two devices and relied on a climate change scenario [46]. Furthermore, to date, there are no studies evaluating *WEC* performance in the six concession zones designated by the Portuguese government for offshore renewable energy projects.

Against the foregoing backdrop, the goal of this study is to address these gaps by evaluating the effectiveness of different *WEC*s for offshore wave energy exploitation in mainland Portugal and conducting a detailed performance analysis of specific *WEC*s within the six concession zones. For this purpose, a 44-year hindcast obtained from a high-resolution *SWAN* numerical model, which was successfully calibrated and validated in Refs. [2,47,48], was used to determine key performance indicators of WEC performance. The remainder of this paper is structured as follows: Section 2 details the materials and methods used in this research. Section 3 presents the results and discusses the key findings. Finally, conclusions are drawn in Section 4.

2. Materials and methods

This study used advanced computational techniques to thoroughly investigate Portugal's entire coastal region using the SWAN (Simulating WAves Nearshore) model [49]. It is worth noting that the model was implemented following the recommendations set by the IEC technical specification for wave energy resource assessment [50], which has proven to be a robust methodology for obtaining accurate wave resource characterizations [51]. Therefore, the model was forced with wind data from the ERA5 reanalysis dataset. This highly reliable dataset provides hourly wind fields at 0.25° resolution, which is essential for improving and verifying wave climate hindcasts [52]. Furthermore, the data collected from the ERA5 wave hindcast reanalysis, at 1° spatial resolution [53], were used as wave boundary conditions for the SWAN model. The

Table 1
Wave energy test facilities worldwide [14].

Test sites	Scale	Wave Resource (kW/m)	Grid Connection	Distance from Shore	Water Depth
Danish Marine Test Site (DanWEC), Denmark [15]	Full	5	Yes	200 m	12 m
Wave Hub, England [16,17]	Full	20	Yes	16 km	55–65 m
SEM-REV, France [18,19]	Full	15	Yes	15 km	35 m
Atlantic Marine Energy Test site, Ireland [20]	Full	70–75	Yes	10 km	100 m
		55–60		6.5 km	50 m
Runde Island, Norway [21]	Full	N/A	Yes	500 m	30–35 m
Pilot zone, Portugal [22]	Full	32	Yes	5–8 km	30–90 m
European Marine Energy Centre, Scotland [23]	Full	22–25	Yes	1–2 km	20–75 m
Biscay Marine Energy Platform (Bimep), Spain [24]	Full	21	Yes	1.7 km	50–90 m
Plocan, Canary Islands, Spain [25,26]	Full	8–10	Yes	2 km	30–1000 m
Nissum Bredning, Denmark [27]	1:4–1:10	$H_{m0} = 1.2$ m	Yes	200 m	4–10 m
The Galway Bay Wave Energy Test Site, Ireland [28]	1:3–1:5	3	No	2.4 km	21–24 m
European Marine Energy Centre, Scotland [14]	1:10	$H_{m0} \sim 0.35$ m	Yes	500 m	21–25 m
Falmouth Bay test site, England [29]	N/A	N/A	No	3–5 km	20–50 m
Pacific Marine Energy Centre USA [30,31]	Full, Large, Small	>15 kW/m	Yes	16 km	100 m
The Hawai'i Wave Energy Test Site, USA [32]	Large	N/A	No	N/A	–
Shandong Test Site, China [33]	Large	4 kW/m	Yes	30 m	–

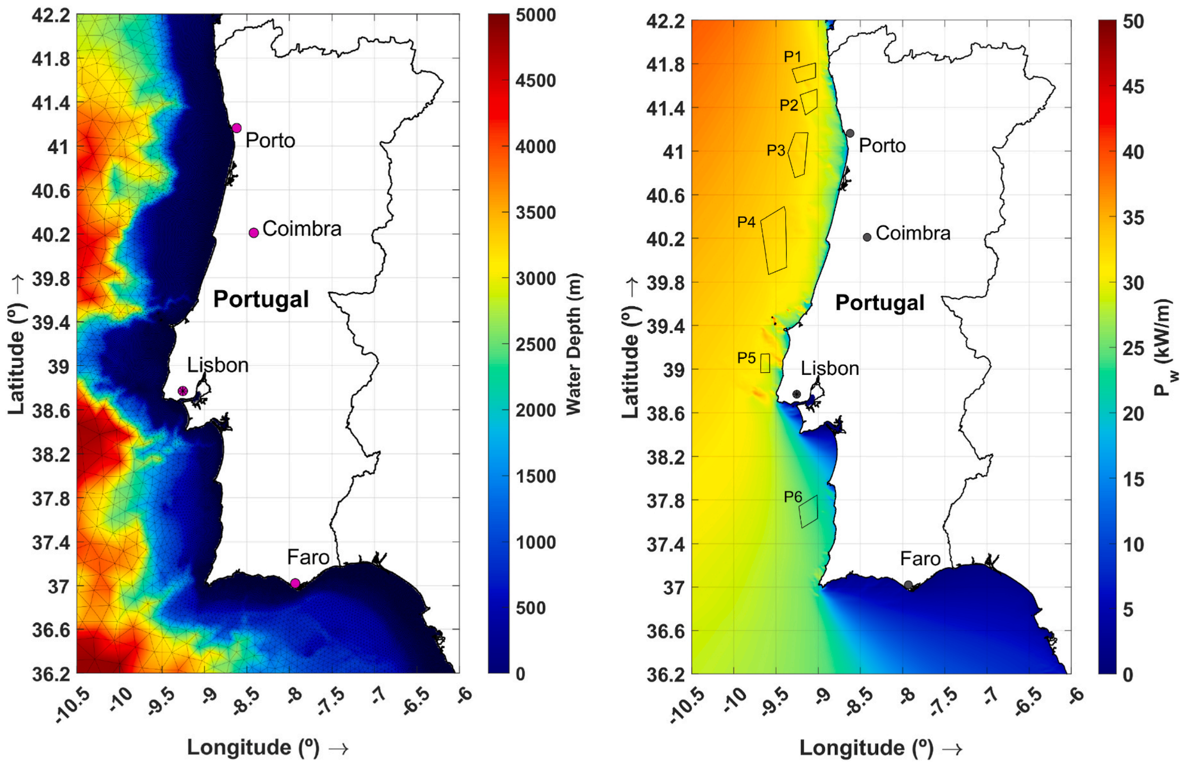

Fig. 1. Study area and bathymetry overlapped by the unstructured mesh utilized in the model (left) and 44-year mean P_w distribution with identification of the six Portuguese concession zones (right).

bathymetric data is based on the General Bathymetric Chart of the Oceans (GEBCO) [54] and is included in the model onto an unstructured mesh with cell sizes ranging from 250 m to 30 km. The finer resolutions are found nearshore to capture relevant bathymetric details. This unstructured mesh (Fig. 1) with 114,518 elements was created using the ADCIRC software [55]. This mesh ensured computational efficiency in areas with a more uniform environment while enabling a detailed depiction of places with significant bathymetric fluctuations [56–58].

In accordance with prior research in the area, the SWAN model was operated in a non-stationary mode, utilizing a JONSWAP spectrum with a peak enhancement factor set at 3.3. The simulations were carried out at hourly intervals and covered 44 years, from 1979 to 2022. Outputs have been produced at the lower temporal resolution of 2 h to manage data volume and space constraints. The model calibration and validation, as presented in Refs. [47,59], involved comparison with data from 10 wave buoys managed by the Portuguese Hydrographic Institute and the Spanish Port Authority, ensuring fidelity in depicting the observed wave climate. Parameters such as the energy wave period (T_e), significant wave height (H_{m0}), and the power per unit length of the wavefront (P_w) are crucial for characterizing wave conditions and are provided as output by the SWAN model.

The scatter diagram and the power matrix categorize data into distinct and ideally consistent classes, offering structured insights into wave resource and *WEC* performance, respectively. The scatter diagram illustrates the joint probability distribution of wave heights (typically, H_{m0}) and periods, thereby indicating the frequency of the different sea states. Conversely, the power matrix specifies the power generated by a particular *WEC* for a given combination of wave height and period. By integrating these two elements, it is possible to estimate a *WEC*'s energy production (E_T) at a particular site during a specific period of time (T). To compute the energy production, the probability distribution of wave heights and periods is first derived from wave models or wave buoy measurements (if available). This distribution is then multiplied (element-wise) by the power matrix corresponding to the specific *WEC*, yielding a matrix of energy production values across various sea states. Subsequently, the total energy production is determined by summing these values in the energy production matrix, weighted by their respective probabilities as given by Ref. [60],

$$E_T = \sum_{i=1}^{nT} \sum_{j=1}^{nH} f_{ij} \, P_{ij} T \tag{1}$$

where f_{ij} represents the percentage of occurrence of wave energy for a specific combination of wave period (i) and wave height (j), and P_{ij} the power generated by the *WEC* for a specific combination of wave period (i) and wave height (j). The value of f_{ij} is obtained from the wave scatter diagram calculated over the period T at the chosen location, while the P_{ij} is obtained from the power matrix of the *WEC*. The values of nT and nH represent the total number of wave period and wave height classes, respectively [60]. Finally, in the present work, E_T is referred to as Annual Energy Production (AEP) or Monthly Energy Production (MEP) when T corresponds to an annual or monthly period, respectively.

The capacity factor, c_f, is one of the most important parameters for understanding the performance of *WEC* concerning power production since it shows how much of the device's overall capacity is utilized to produce electricity in a given situation. It also displays the ratio of full running load hours over time. The capacity factor can be calculated using [61,62],

$$c_f = \frac{P_E}{P_r} \tag{2}$$

where P_r is the rated power of the *WEC* and P_E is the expected wave power output of the *WEC* for the defined period.

Another important parameter is the capture width (c_w) in meters. This parameter is commonly used as a proxy for wave power capture. It is also known as the wave-front width, which may be used to extract all of the absorbed power by *WEC*s. It is given by Ref. [61],

$$c_w = \frac{P_E}{P_w} \tag{3}$$

The P_w in the present study was directly the resultant of P_x and P_y components of the energy transport per meter of the wave front in both directions [49],

$$P_w = \sqrt{{P_x}^2 + {P_y}^2} \tag{5}$$

$$P_x = \rho g \iint c_x E(\omega,\theta) d\sigma d\theta \text{ and } P_y = \rho g \iint c_y E(\omega,\theta) d\sigma d\theta \tag{6}$$

where ρ represents the water density (in kg/m^3), g denotes the gravity constant (in m/s^2), c_x and c_y stand for the x and y components of the group velocity of waves (in m/s), $E(\omega,\theta)$ denotes the wave spectrum, depicting the energy density of waves at frequency ω and direction θ, σ serves as an integration variable representing frequency within the wave energy spectrum, and ω represents the intrinsic angular frequency of the waves, defined as $\omega = 2\pi f$, where f is the frequency in Hz.

This study undertakes a complete evaluation of multiple *WEC* technologies deployed offshore the coast of mainland Portugal, focusing on their spatial and temporal performance in terms of E_T, c_f, and c_w. Monthly- and annual-based analyses are considered in order to capture trends in seasonal and yearly fluctuations. Table 2 provides an overview of the main characteristics of the considered *WEC* technologies, whose power matrices were available. These characteristics include rated power output, classification, installation depth, and power matrix classes. The assessed *WECs* varied from point absorbers like AquaBuoy and AWS to bottom-fixed systems such as HeaveBuoy. Each *WEC* is designed for a specific optimal deployment environment varying from offshore to nearshore and shallow waters. The power matrices, with bin classes defined by the significant wave height (H_{m0}) and either peak period (T_p) or energy period (T_e) of the devices highlighted in Table 2, are presented in Appendix A. It is worth noting that while power matrices were available for the considered *WEC* technologies, some of these technologies are no longer in use. Therefore, the applicability of the results may vary depending on the current state of the technology and its relevance to contemporary wave energy projects.

Finally, Table 3 provides detailed information on the six concession zones designated by the Portuguese government for offshore renewable energy extraction. Each zone is mostly characterized by its distance to the shore and estimated wave potential. The geographical coordinates are included for the representative center point locations, denoted as P1 to P6, of the associated zone. The mean and standard deviation (Std) of potential P_w presents insights into the variability of the energy resources at representative locations. Additional details such as water depth from mean sea level and distance to the shore offer crucial insight into possible environmental and operational conditions within each concession zone.

3. Results and discussion

As indicated in the previous section, the procedure to assess the performance of case-study *WECs*, chosen for their ability to operate in offshore environments and well-documented power matrices in the literature, was based on metrics such as *AEP*, c_f, and c_w. The spatial distributions of those metrics were examined along the whole coast of the study area, with particular emphasis on the six designated concession zones (P1-P6) for offshore renewable energy extraction. Additionally, scatter diagrams provided insight into the wave resources at representative locations, while heatmaps depict the mean monthly wave energy flux variation over 44 years. Monthly changes in mean electricity production and c_f for selected *WECs* across the six locations were also analyzed, shedding light on their performance dynamics throughout the year. These analyzes provide a comprehensive understanding of individual *WEC* performance operating in diverse environmental conditions, offering valuable insight for future wave energy initiatives.

3.1. Wave resource characterization

Wave resource characterization is essential for optimizing the deployment of *WECs*. Understanding the spatial and temporal variations in wave energy helps in identifying the most promising locations for energy extraction and designing efficient *WECs* tailored to specific environmental conditions. Fig. 1 provides a comprehensive view of the study area along the coast of Portugal, combining bathymetric data and wave power distribution.

The left plot of Fig. 1 illustrates the study area's bathymetry overlaid with the unstructured mesh used in numerical modeling, with the mesh density higher near the coastline, indicating greater resolution in these areas. Key cities such as Lisbon, Porto, Coimbra, and Faro are marked for reference. The right plot of Fig. 1 displays the 44-year mean P_w, revealing that the highest wave power is concentrated along the northern and central coast (with values up to 35 kW/m), while the southern coast exhibits significantly lower values (in the order of 10 kW/m). Additionally, the six concession zones designated by the Portuguese government for offshore renewable energy extraction are shown as polygons labeled P1 to P6 on the right side of Fig. 1.

The monthly mean P_w variations in the six designated concession zones (P1 to P6) are critical for understanding the temporal distribution of wave energy resources, informing the optimal deployment and operation of offshore renewable energy systems in each zone. The heatmaps of the P_w during 44 years against the 12 months for P1, P3 and P5 locations are plotted in Fig. 2 (P2, P4 and P6 are presented in Fig. D1, Appendix B).

The analysis of P_w data across locations P1 to P6 in Fig. 2 and Fig. B1,

Table 2
Main characteristics of the considered *WEC* technologies [63–66].

No	*WECs*	Nominal power [kW]	Classification	Operation depth range [m]	Power matrix classes [m × s]	
1	CorPower	750	Point absorber	Offshore (>40)	0.5 × 1.0	[$H_{m0} \times T_p$]
2	AquaBuoy	250	Point absorber	Offshore (>50)	0.5 × 1.0	[$H_{m0} \times T_p$]
3	AWS	2470	Point absorber	Offshore (40–100)	0.5 × 0.5	[$H_{m0} \times T_e$]
4	OEBuoy	2880	Point absorber	Offshore (>100)	0.5 × 1.0	[$H_{m0} \times T_p$]
5	Pontoon	3619	Point absorber	Offshore (>100)	0.5 × 1.0	[$H_{m0} \times T_p$]
6	Langlee	1665	Oscillating surge transducer	Offshore	0.5 × 1.0	[$H_{m0} \times T_p$]
7	CETO	260	Point absorber	Nearshore (20–50)	0.5 × 1.0	[$H_{m0} \times T_e$]
8	Oyster 2	3332	Point absorber	Nearshore (<50)	0.5 × 1.0	[$H_{m0} \times T_e$]
9	Oyster	290	Terminator	Nearshore (10–25)	0.5 × 1.0	[$H_{m0} \times T_e$]
10	Seabased AB	15	Absorber	Nearshore (30–50)	0.5 × 1.0	[$H_{m0} \times T_p$]
11	SSG	20000	Terminator	Foreshore	0.5 × 0.5	[$H_{m0} \times T_e$]
12	HeaveBuoy	2192	Bottom-fixed	Shallow water	0.5 × 1.0	[$H_{m0} \times T_e$]
13	Oceantec	500	Absorber	Offshore (30–50)	0.5 × 1.0	[$H_{m0} \times T_p$]
14	WaveStar	2709	Point absorber	Nearshore (30–50)	0.5 × 1.0	[$H_{m0} \times T_e$]
15	PWEC	480	Oscillating body	Nearshore (10–50)	1.0 × 2.0	[$H_{m0} \times T_p$]
16	Pelamis	750	Absorber	Offshore (50–70)	0.5 × 0.5	[$H_{m0} \times T_e$]
17	WaveBob	1000	Point absorber	Offshore (>50)	0.5 × 0.5	[$H_{m0} \times T_p$]
18	WaveDragon	7000	Terminator	Nearshore (30–50)	0.5 × 0.5	[$H_{m0} \times T_e$]

Table 3
Characterization of the six concession zones for offshore renewable energy extraction by the Portuguese government, adapted from Ref. [34].

Regions	Distance to shore (km)	Area (km^2)	Expected potential (GW)	Label	Lon (°)	Lat (°)	Mean P_w (kW/m)	Std of P_w (kW/m)	Distance to shore (km)	Water depth (m)
Viana do Castelo Norte	7–19.5	312	1.09	**P1**	−9.1611	41.7116	32.3	40.2	13	111
Viana do Castelo Sul	10.5–17.9	294	1.03	**P2**	−9.1010	41.4676	30.7	42.1	14	104
Leixões	22.5–32.3	644	2.0	**P3**	−9.2434	40.9703	32.3	30.8	27	150
Figueira da Foz	21.7–34.1	1325	4.0	**P4**	−9.5191	40.1715	32.3	40.5	28	160
Ericeira	7.5–12.4	171	0.5	**P5**	−9.6341	39.0563	29.5	43.7	10	98
Sines	9.8–19.3	430	1.5	**P6**	−9.1086	37.6888	24.5	34.5	15	332

Appendix B reveals several commonalities and variations, providing valuable insight into oceanic conditions across the concession zones. A clear seasonal trend is observed across all locations, with winter (Dec, Jan, and Feb) consistently exhibiting the highest mean P_w, followed by autumn (Sep, Oct, and Nov). Winter mean P_w ranges from 42.8 kW/m in location P6 to 58.9 kW/m in location P1. Spring (Mar, Apr, and May) and summer (Jun, Jul, and Aug) generally exhibit lower mean P_w values compared to winter and autumn months, with values ranging from 9.3 to 30.6 kW/m. This pattern of stronger wave activity during colder seasons is influenced by atmospheric and oceanic dynamics, with the North Atlantic Oscillation (*NAO*) playing the most significant role, alongside the East Atlantic (*EA*) and Scandinavia (SCAND) patterns [67]. The *NAO* is a large-scale atmospheric oscillation characterized by fluctuations in the pressure difference between the Icelandic Low and the Azores High [68]. Thus, the *NAO* plays a pivotal role in steering storm trajectories across the North Atlantic. The *NAO* index, indicating this oscillation, alternates between positive and negative phases, associated with a strong or weak pressure contrast between these regions, respectively. When the *NAO* index is positive, intensified winter storms tend to move northeastward across the Atlantic, generating high-energy waves predominantly from the northwest, particularly impacting the northern Iberian coast [69]. Conversely, negative *NAO* phases result in weaker and less frequent storms, with mid-latitude storm tracks shifting eastward, causing a more uniform wave climate along the Iberian Atlantic coast as wave directions become more westerly [70]. Similar to the *NAO* index, positive phases of the East Atlantic (*EA*) pattern contribute to the generation of northwest-oriented swells [71]. Over the past 25 years, a trend toward positive *NAO* and *EA* values has been observed, contributing to increasingly intense wave conditions [72,73].

Year-to-year variability in P_w is also evident, with some years experiencing heightened wave activity compared to others. Notably, 2014 stands out as the year with the highest mean P_w across all locations. Under positive phases of *NAO* and *EA* indices (exceeding values of 1 [74,75]) the 2014 winter was characterized by a continuous cluster of extreme storm events occurring every 48–72 h [76]. This led to some of the highest winter wave energy levels recorded along the East Atlantic coast at mid and southern latitudes (38°N–55°N) over the past seven decades [77]. Conversely, the years 2005 and 2010, which featured negative phase values of *NAO* and *EA* [75], presented significantly lower mean P_w values, ranging from 27 to 36 kW/m, indicating the strong influence of atmospheric teleconnection patterns in the region [36].

Extremes in P_w, represented by maximum and minimum months exhibit high variability within and across years at all locations. February 2014 consistently emerges as the month with the highest mean P_w, while July 2013 consistently exhibits the lowest mean P_w. The maximum mean P_w ranges from 112 kW/m in location P6 to 142.6 kW/m in location P1, whereas the minimum mean P_w ranges from 4.3 kW/m in location P6 to 6 kW/m in location P4. These extremes underscore the dynamic nature of P_w variability and stress the importance of understanding both seasonal and yearly fluctuations. Furthermore, location P1 exhibits the highest volatility in P_w among the six, with a wide range of values observed across seasons and years. Conversely, concession zone P6 shows the least volatility, with a narrower range of mean P_w values.

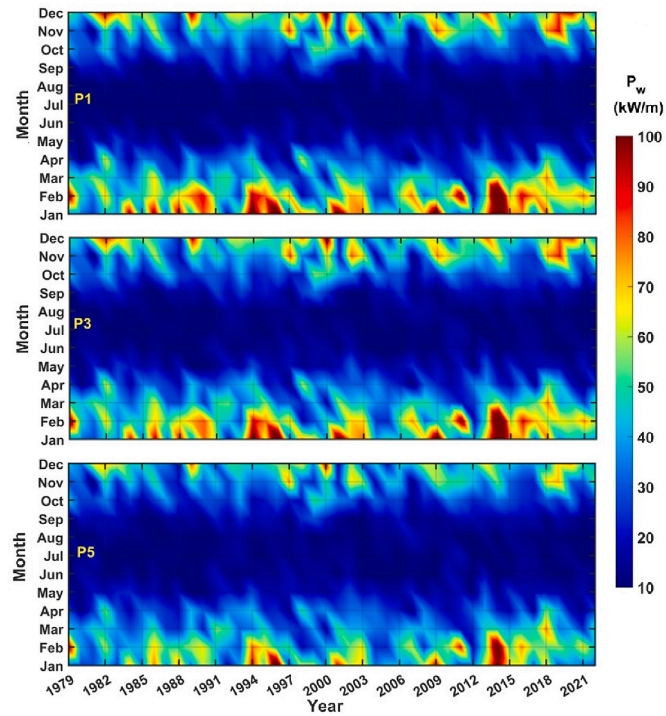

Fig. 2. Mean monthly power variations across 44 years in three representative locations in the center of the concession zones designated by the Portuguese government for P1, P3 and P5.

Overall, while each location exhibits unique characteristics and variations in P_w, common patterns such as seasonal variations and yearly trends are evident. Understanding these patterns is crucial for applications like coastal management, offshore engineering, and renewable energy development, emphasizing the importance of comprehensive analyses and monitoring of oceanic conditions.

The scatter diagrams in Fig. 3 offer a detailed view of the mean annual energy distribution across the six concession zones. These diagrams, employing energy bin sizes of 2 s for T_p and 1.0 m for H_{m0}, provide valuable insights into the frequency and total energy delivery for various sea states on an annual basis. Notably, the color map within each diagram visually represents the yearly energy output in MWh/m for different sea state combinations, while the number of hours denotes the frequency of occurrence for each specific condition. Analyzing the plots in Fig. 3 individually, intriguing similarities and differences across the locations are observed. For example, P1 exhibits a predominant energy concentration within the 12–16 s T_p range and 2–5 m H_{m0} range, translating to substantial P_w levels of 20–200 kW/m. With a peak energy delivery of 32.4 MWh/m/year, this location demonstrates robust potential for wave energy extraction, particularly in sea states characterized by approximately 13 s of T_p and 2.5 m of H_{m0}. Moving to P2, P3, P4, P5, and P6, a recurring pattern of high energy concentration within similar sea state ranges – aligning closely with P1's findings – is noted.

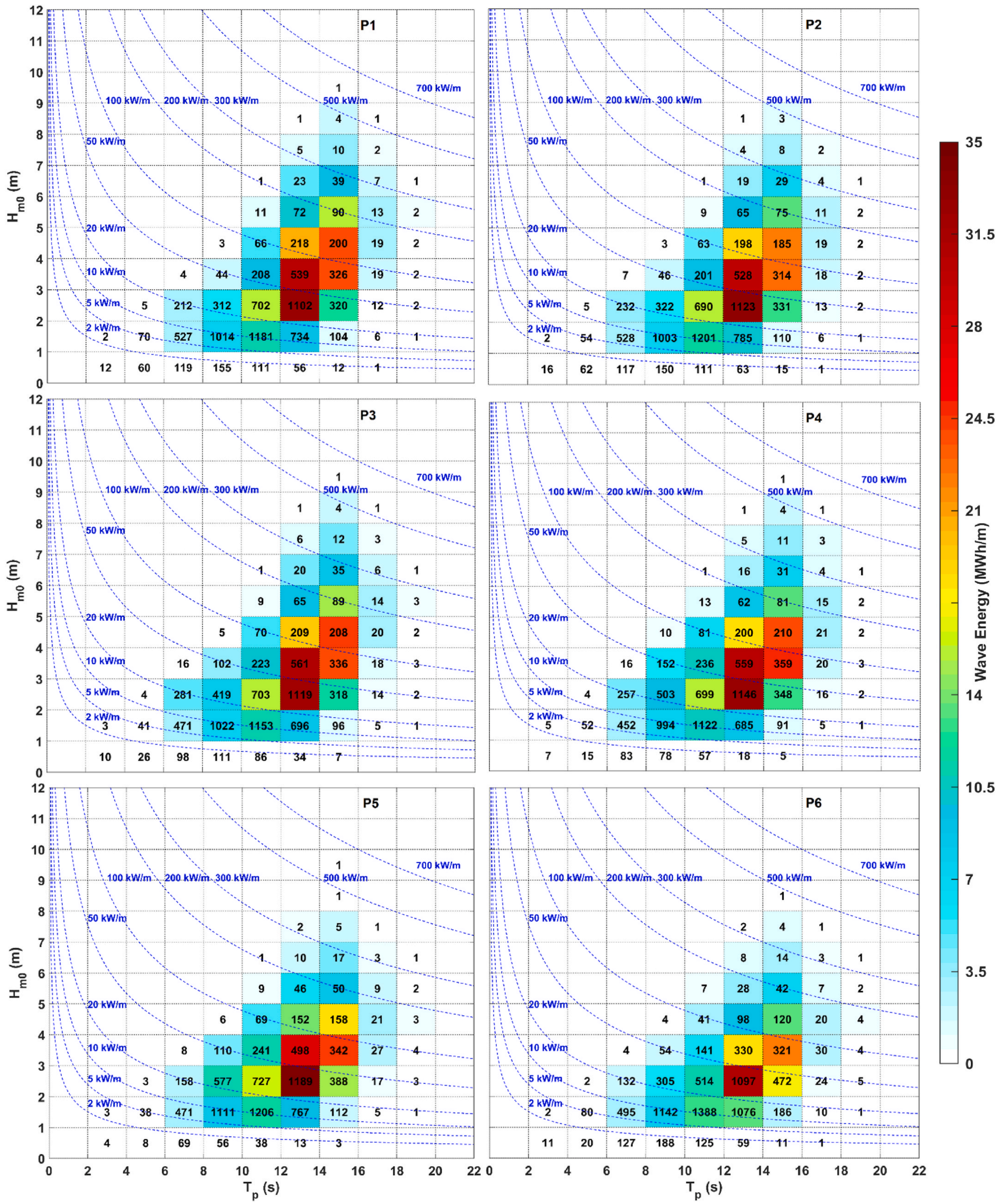

Fig. 3. Scatter diagrams of the wave resources at the six representative locations in concession zones designated by the Portuguese government labeled as P1 to P6.

These locations also showcase significant P_w potential in the range of 20–100 kW/m, with a maximum annual energy resource ranging from 31.1 to 34.1 MWh/m/year. However, subtle differences in the exact T_p and H_{m0} combinations contribute to the differences found in energy distribution and frequency of occurrence among these locations. The number of sea state occurrences among the bins, changes in each

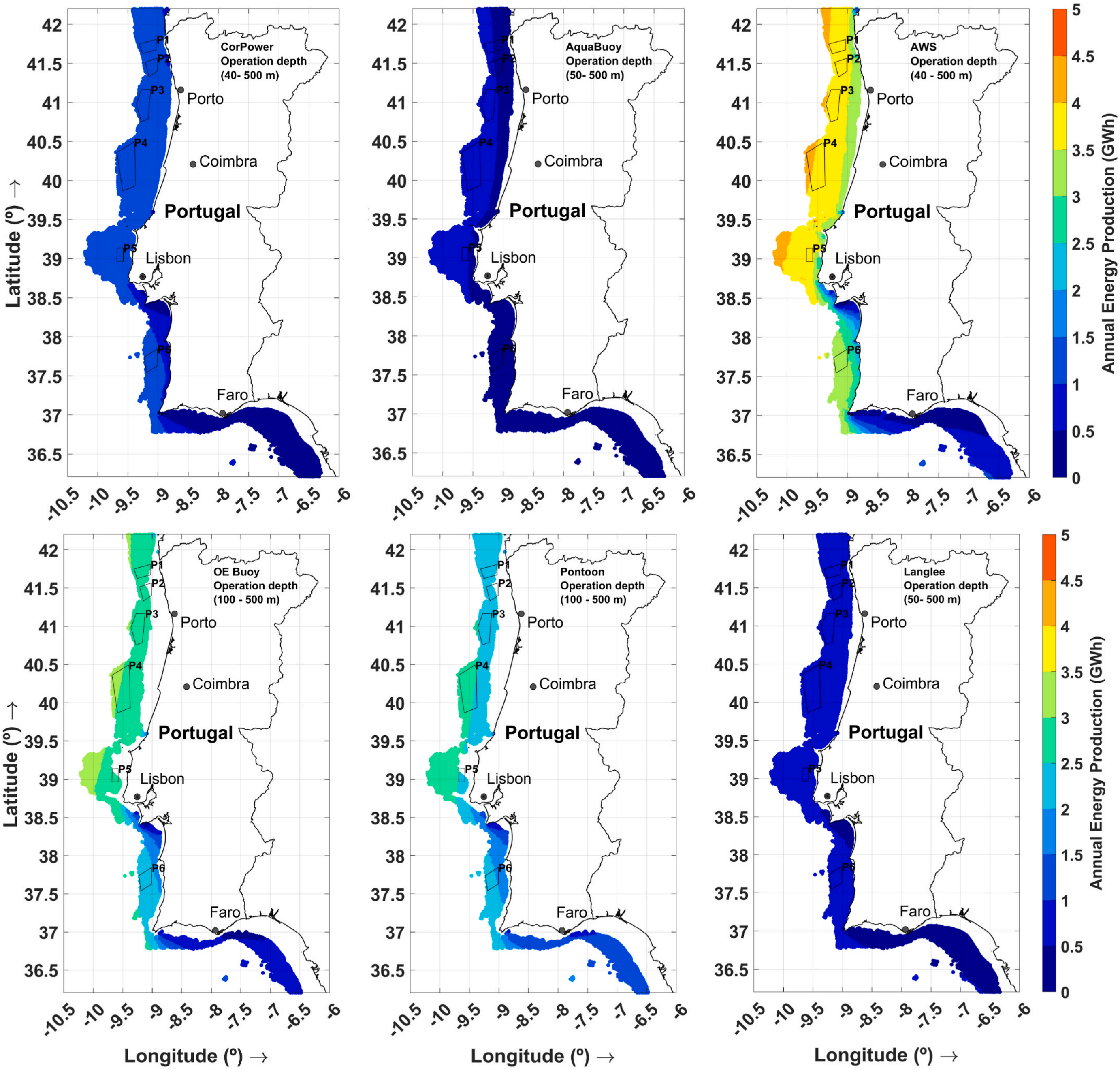

Fig. 4. Spatial distributions of mean annual energy production (*AEP*) for CorPower, AquaBuoy, Langlee, Pontoon, OEBuoy and AWS *WECs* in their operation depth range.

location, reflecting the uniqueness of the local wave climate and hydrodynamic conditions at each site. This outcome can be used in designing the natural period of the Power Take-Off systems of resonant wave energy converters, allowing for the optimization of energy conversion efficiency and system performance. Finally, Appendix C provides the monthly scatter diagrams for the six concession zones, enabling an assessment of wave energy distribution and the frequency of various sea states over the course of the year.

3.2. Wave energy Converter performance assessment

Figs. 4–6 present the performance across the Portuguese coast of six selected *WEC* technologies—CorPower, AquaBuoy, AWS, OEBuoy, Pontoon, and Langlee. These technologies were chosen for two main reasons: first, they are capable of operating in offshore environments at the depth characteristic of the six concession zones under this study; second, their power matrices are well-documented and available in the literature, providing a reliable basis for performance comparison and analysis.

The spatial distributions of annual energy production (*AEP*) for CorPower, AquaBuoy, AWS, OEBuoy, Pontoon, and Langlee *WECs*, as depicted in Fig. 4, reveal distinct performance patterns along the Portuguese coast. For CorPower, the *AEP* values display a pronounced northward increase, with zones P4 and P5, situated north of Lisbon, achieving the highest energy outputs, exceeding 1.33 GWh. AquaBuoy identifies zones P3 and P4, also north of Lisbon, as the most favorable locations, with *AEP* values surpassing 0.53 GWh. For AWS, the highest *AEP* values are observed in the northern and central zones, specifically P1 to P4, where they range from 3.87 GWh to 3.98 GWh. Among these, zone P4, located off the coast of Figueira da Foz, stands out with the

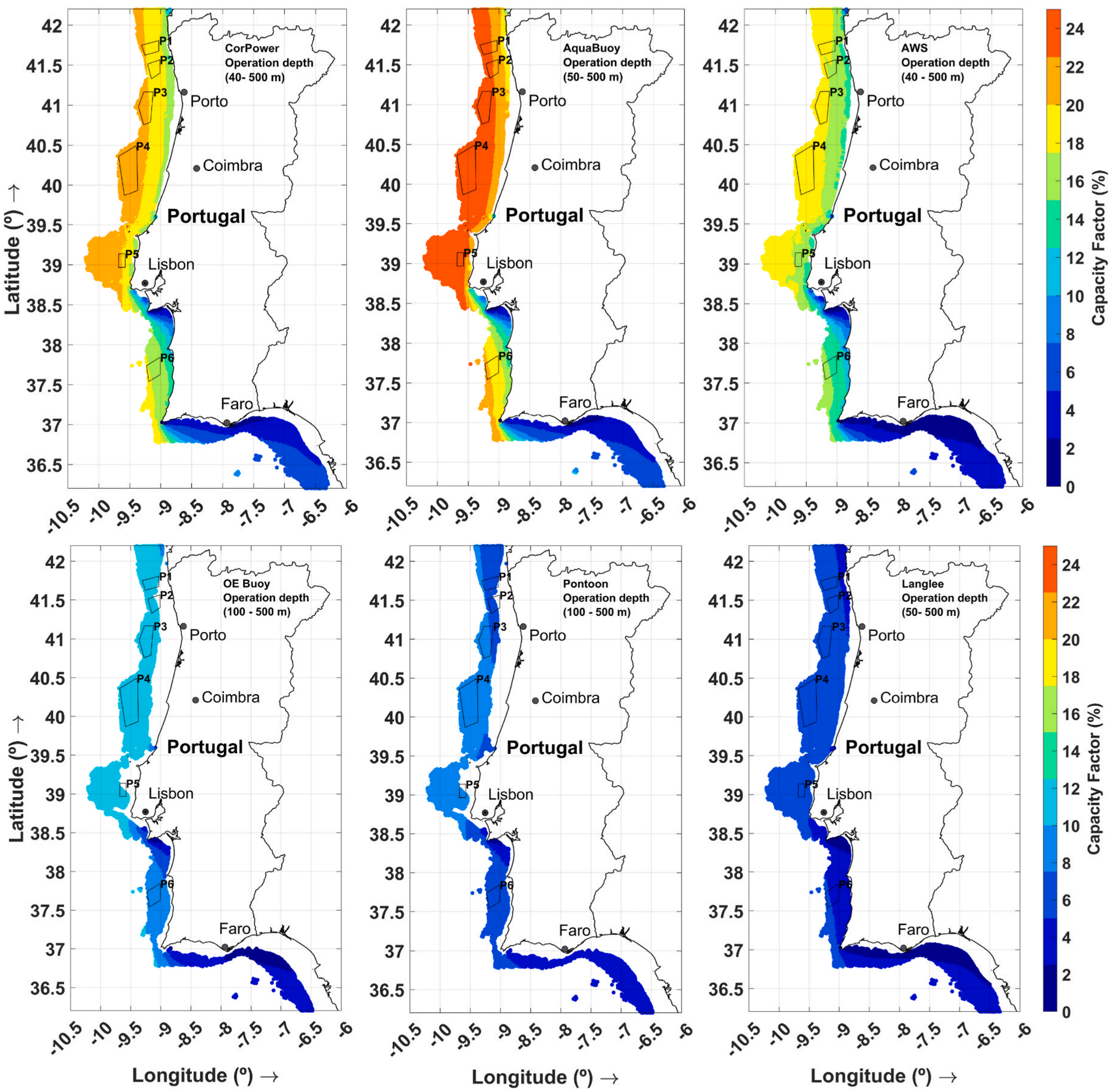

Fig. 5. Spatial distributions of capacity factor (c_f) for CorPower, AquaBuoy, Langlee, Pontoon, OEBuoy and AWS *WECs* in their operation depth range.

maximum *AEP* of 3.98 GWh. The OEBuoy demonstrates a similar trend, with zones P3 and P4 recording the highest *AEP* values, both exceeding 2.9 GWh, with a peak of 2.99 GWh in zone P4. The Pontoon *WEC* exhibits performance comparable to that of the Langlee device, with zones P3, P4, and P5, situated between Lisbon and Porto, emerging as the most productive site. In these zones, the *AEP* values exceed 2.4 GWh, with zone P4 reaching a peak of 2.56 GWh. Finally, the Langlee *WEC* achieves its highest *AEP* values in zones P3, P4, and P5, surpassing 0.85 GWh, with zone P4 standing out at 0.91 GWh. These results underscore the central and northern zones, particularly zone P4, as consistently offering the most favorable conditions for wave energy production across all six WEC technologies analyzed.

Fig. 5 illustrates the capacity factor (c_f) values for the six Wave Energy Converters (*WECs*), highlighting notable spatial trends along the Portuguese coast. CorPower demonstrates a peak c_f of 20.82 % in zone P4, strongly indicating the central and northern zones as optimal locations for deployment. Similarly, AquaBuoy achieves its highest c_f values, surpassing 24 %, in zones P3 and P4, further emphasizing the suitability of these areas for efficient energy conversion. For AWS, the c_f values exceed 17.3 % across zones P1 to P4, with a maximum value of 18.4 % recorded in zone P4. The performance of OEBuoy aligns with this trend, reaching its highest c_f of 11.5 % in the same zone. The Pontoon *WEC* also exhibits its best performance in zone P4, attaining a maximum c_f of 8.06 %. Langlee follows a similar pattern, with its highest c_f of 6.22 % observed in zone P4 as well. These results consistently highlight zone P4 as offering the most favorable conditions for energy efficiency across all six WEC technologies considered in this study. The notable clustering of peak c_f values in zone P4 underscores its optimal suitability for large-scale deployment of wave energy converters, particularly at the operational scale examined.

The capture width (c_w) values shown in Fig. 6 reveal a different spatial trend to *AEP* and c_f. For CorPower and AquaBuoy, the highest c_w values are observed in zone P6 in the south, indicating higher potential for energy capture in these regions. Similarly, AWS and OEBuoy show their highest c_w values in zones P5 and P6, despite these zones having lower *AEP* and c_f values. For the Pontoon WEC, zones P5 and P6 exhibit the highest c_w values, reflecting efficient energy capture in southern zones. Finally, the Langlee *WEC* shows its highest c_w values along the coast of Faro city in the south, although these remain relatively consistent across all zones at approximately 0.2 m, indicating lower efficiency compared to the other *WECs* analyzed.

The comprehensive analysis of spatial distributions of *AEP*, c_f, and c_w for six different wave energy converters (CorPower, AquaBuoy, AWS, OEBuoy, Pontoon, and Langlee) along the Portuguese coast consistently

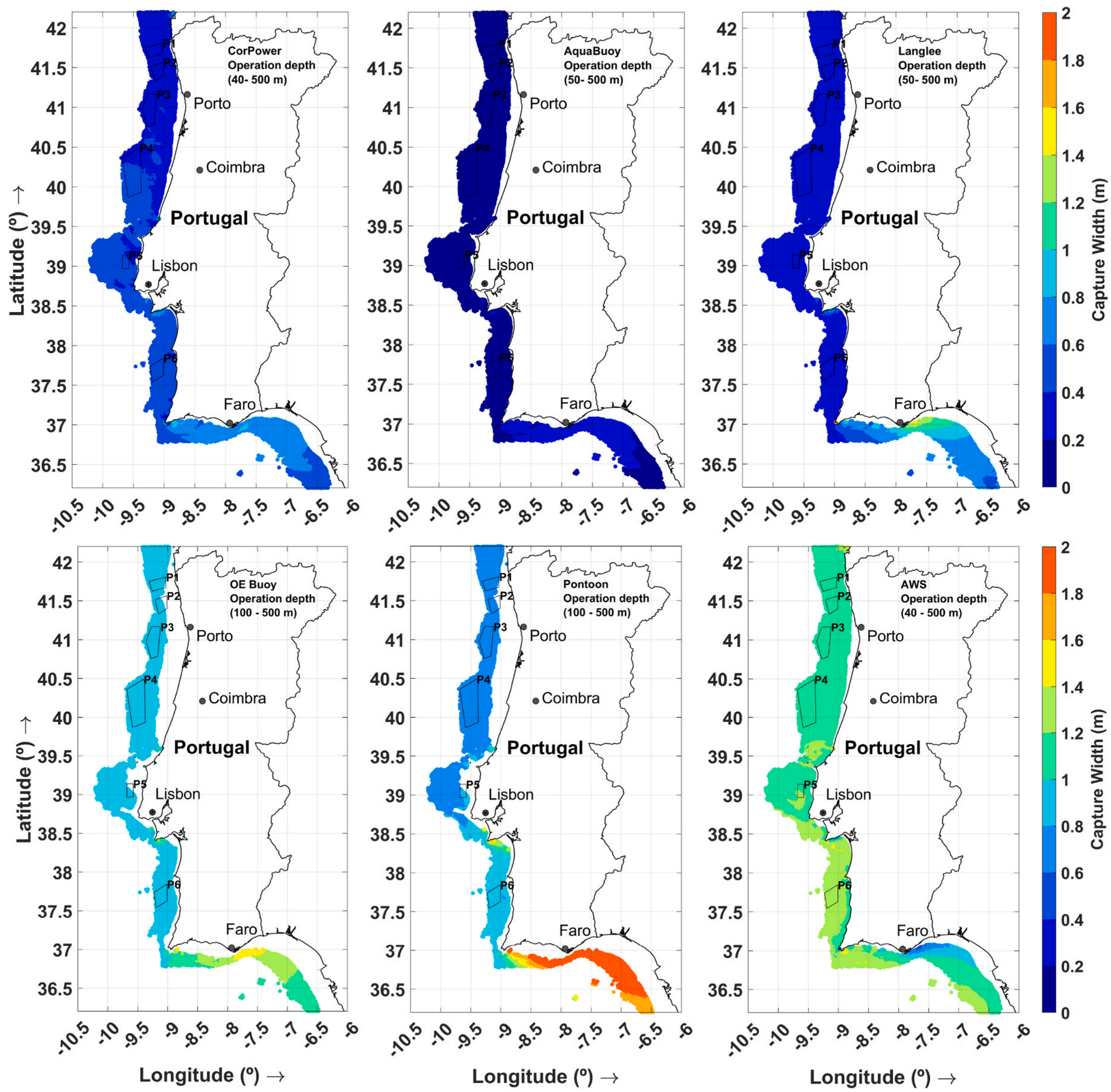

Fig. 6. Spatial distributions of capture width (c_w) for CorPower, AquaBuoy, Langlee, Pontoon, OEBuoy and AWS *WECs* in their operation depth range.

highlight zone P4 as the optimal site for the full-scale *WEC* technologies considered in this study. This zone, located north of Lisbon, presents the highest energy production and efficiency across all *WEC* types, with notable peaks in *AEP* and c_f, particularly for CorPower, AquaBuoy, AWS, and OEBuoy. Zones P3 and P5 also show favorable conditions, though to a slightly lower extent, making them viable alternatives for *WEC* installations. In contrast, the southern zones particularly zones P5 and P6, exhibit higher c_w but lower overall c_f and *AEP*, suggesting they are less suitable for large-scale wave energy farms. Notably, the rated power of the considered WEC technologies, particularly the Pontoon and Langlee devices, appears to be oversized for the wave conditions along the Portuguese coast. To enhance their efficiency, it is necessary to optimize their PTO systems accordingly. This spatial analysis underscores the importance of a balanced approach that considers *AEP*, c_f, and c_w to identify optimal deployment sites. In addition to the performance analysis of the six selected *WEC* technologies in Figs. 4–6, detailed information on an additional 12 WECs (CETO, Oyster 2, Oyster, Seabased AB, SSG, Bottom Fixed HeaveBuoy, Oceantec, WaveStar, PWEC, Pelamis, WaveBob, and WaveDragon) is provided in Appendix D. These 12 WECs were not included in the main analysis due to space limitations and their operation depth does not extend to the offshore renewable energy concession zones targeted in this study.

Fig. 7 presents a detailed analysis of the monthly energy production (MEP) and c_f for six different *WECs* across six locations. The energy output at P4 with the best performance ranges from 36 to 579 MWh, and the c_f varies from 5.2 % to 31.8 %. Conversely, location P6 consistently exhibits the lowest performance, with energy output ranging from 26 to 497 MWh and capacity factors between 3.8 % and 27 %.

In Fig. 7, CorPower technology shows a peak in energy output during the winter months at all locations, with P4 providing the highest energy production and c_f, while P6 displays the lowest values. AquaBuoy exhibits significant seasonal variation with higher outputs in winter, particularly in P4, where it peaks around 55 MWh in January. The c_f follows this trend, with P4 outperforming the other locations. AWS stands out as the best-performing *WEC* overall, delivering the highest energy output across all locations, especially at P4, where it reaches up to 579 MWh. OEBuoy also performs well, particularly at P4, maintaining a high energy output consistently throughout the year. Pontoon displays a notable performance in the summer months across all locations, with the highest output in P4. Langlee shows significant monthly

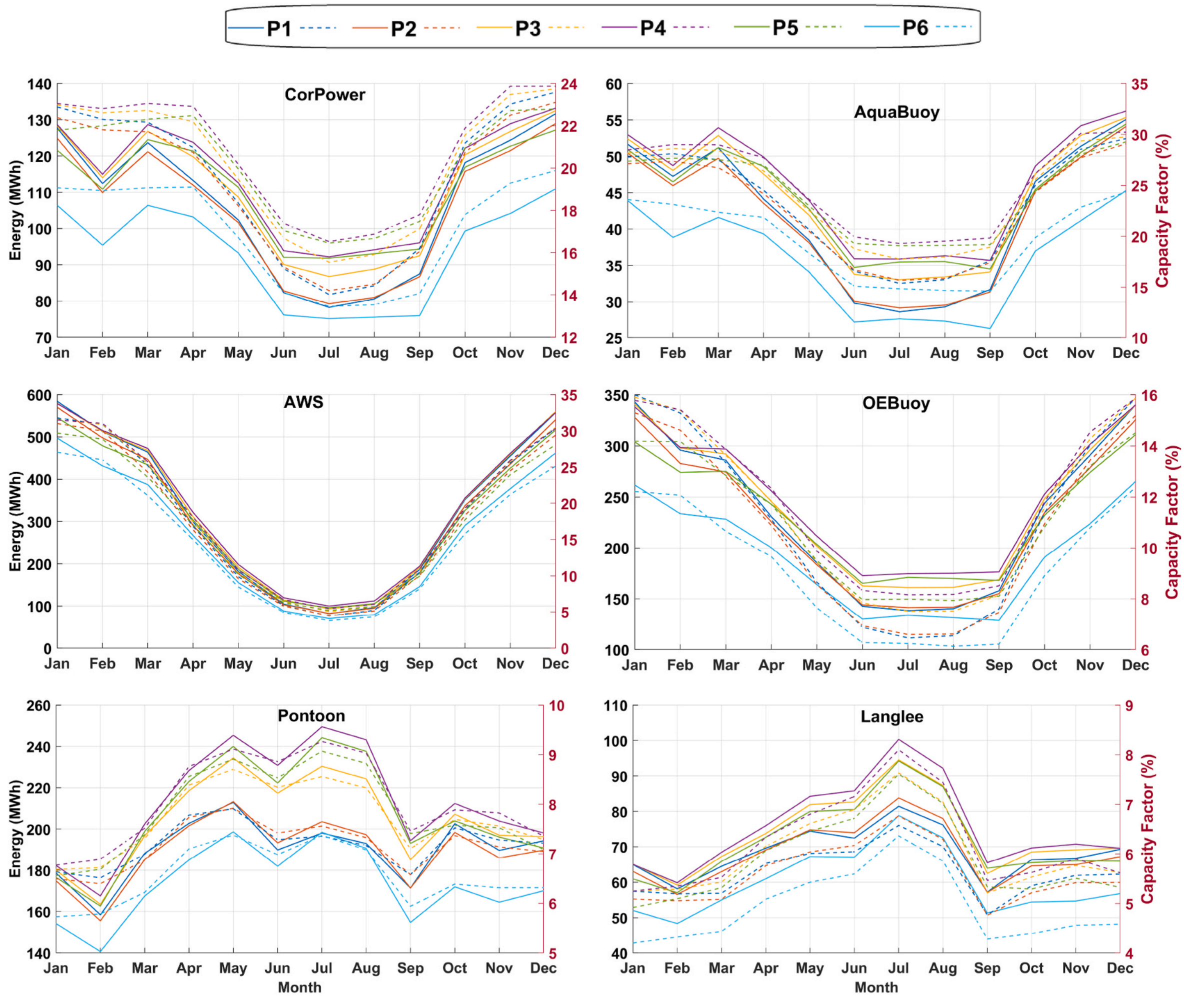

Fig. 7. Monthly variations in the energy production (left y-axis, continuous lines) and capacity factor (right y-axis, dashed lines) of 6 WECs in six representative locations in the center of the concession zones designated by the Portuguese government labeled as P1 to P6.

fluctuations, with higher energy outputs and capacity factors in the summer months.

Location P4 is consistently the best site due to superior wave conditions. AWS emerges as the top-performing *WEC* in terms of mean monthly energy output across all locations, followed by OEBuoy and Pontoon. Langlee and Pontoon, despite lower outputs compared to AWS, show strong summer performance, highlighting their potential to complement winter-peaking *WECs* like AWS and OEBuoy in a diversified wave energy farm. This outcome is attributed to the characteristics of the Langlee and Poonton WECs, whose optimal operating range corresponds to T_P values between 7 and 11 s. These values align with the predominant wave conditions observed from May to August (Fig. C4, Appendix C), characterized by T_P values between 6 and 10 s, associated with wind sea conditions. Conversely, AWS operates optimally within a T_P range of 10.5–14.5 s (Table A3), aligning with swell-dominated winter wave conditions. However, assessing the complementarity of different WECs to achieve more stable energy production would require a comprehensive techno-economic analysis, which lies beyond the scope of this study.

Finally, it is important to note that the performance metrics obtained for the different *WECs* analyzed may be limited, particularly regarding the capacity factor (c_f) and capture width (c_w) parameters. This is primarily because the *WECs* studied are not optimized for the specific wave conditions of Portugal, such as the power capacity and/or resonant periods that match the typical wave periods of the Portuguese wave climate. Consequently, future optimization efforts are necessary to adapt the *WECs* to the characteristics of the Portuguese shoreline, thereby enhancing their efficiency, which will be addressed in future research. Additionally, while this analysis was conducted on the most relevant *WECs* for which power matrices are available (Appendix A), the methodology presented in this paper can be applied to any other *WEC*.

4. Conclusions

This study presents a comprehensive assessment of wave energy potential along the coast of mainland Portugal, with a particular focus on the six designated concession zones for marine renewable energy exploitation. Utilizing advanced computational techniques, the performance of various *WEC* technologies was evaluated to identify optimal deployment areas. The analysis revealed significant wave energy potential, especially highlighting the effectiveness of different *WEC* devices in specific regions and seasons.

The results indicate that point absorbers like AWS and OEBuoy show high energy production potential in offshore locations, while devices such as Pontoon and oscillating surge transducers like Langlee exhibit favorable performance metrics, particularly during the summer months. Spatial mapping of performance metrics identified zones P3 (Leixões) and P4 (Figueira da Foz) as particularly favorable for *WEC* deployment, demonstrating high *AEP*, c_f, and moderate c_w. The study found that the northern regions generally offer higher energy production potential compared to the southern regions. Additionally, a temporal analysis revealed seasonal fluctuations in wave energy flux, with winter months consistently yielding higher mean energy outputs compared to summer months. Notably, Pontoon and Langlee performed better in the summer months, while CorPower, OEBuoy, AquaBuoy, and AWS were more efficient in the winter months. These findings consider the operational months, incorporating the functionality of shutdown and protection mechanisms for survivability. The study also observed year-to-year variations in wave energy resources, underscoring the importance of understanding both seasonal and yearly trends for effective energy forecasting and strategic deployment decisions.

In summary, this study provides valuable insights into the wave energy potential along the Portuguese coast, offering strategic guidance for the development of wave energy projects. While the findings demonstrate the potential for significant contributions to Portugal's renewable energy mix and support the country's ambitions for sustainable energy production, it is crucial to acknowledge that these results are based on current *WEC* technologies that may not be fully optimized for local conditions. This limitation underscores the need for further research and development to tailor *WEC* designs to specific site conditions, ensuring optimal performance in real-world applications. Nonetheless, through continued technological advancements and strategic planning, Portugal can leverage its abundant wave energy resources to play a leading role in global efforts to combat climate change and achieve energy security.

CRediT authorship contribution statement

Ajab Gul Majidi: Writing – original draft, Visualization, Validation, Software, Resources, Methodology, Investigation, Formal analysis, Data curation, Conceptualization. **Victor Ramos:** Writing – review & editing, Visualization, Software, Conceptualization. **Paulo Rosa Santos:** Writing – review & editing, Supervision, Conceptualization. **Luciana das Neves:** Writing – review & editing, Supervision, Conceptualization. **Francisco Taveira-Pinto:** Writing – review & editing, Supervision.

Declaration of competing interest

The authors declare that they have no known competing financial interests or personal relationships that could have appeared to influence the work reported in this paper.

Acknowledgments

The authors acknowledge funding in the form of a Ph.D. scholarship grant by the Portuguese Foundation of Science and Technology (FCT), co-financed by the EU's ESF through the NORTE 2020 program, with reference 2021.04847.BD. Furthermore, during this research study, Victor Ramos was supported by the program of Stimulus of Scientific Employment Individual Support (CEECIND/03665/2018) from the Portuguese Foundation of Science and Technology (FCT).

Appendix A

Table A1
Power matrix for CorPower in kW with the rated power of 750 kW [78].

	T_p (s)											
H_{m0} (m)		**5.0**	**6.0**	**7.0**	**8.0**	**9.0**	**10.0**	**11.0**	**12.0**	**13.0**	**14.0**	**15.0**	**16.0**
	0.5	0	0	20	30	40	43	45	45	38	35	30	25
	1.0	0	10	30	50	65	70	75	80	70	53	50	48
	1.5	0	35	63	90	110	125	140	140	130	100	80	75
	2.0	10	50	88	120	160	180	185	190	180	125	115	105
	2.5	27	80	130	190	225	230	235	240	210	190	165	130
	3.0	45	115	170	240	260	300	310	320	250	217	180	160
	3.5	60	145	230	300	320	330	345	350	300	245	220	190
	4.0	75	160	300	340	365	400	400	400	340	300	240	225
	4.5	85	180	340	380	400	445	440	450	395	320	280	250
	5.0	95	230	380	455	480	490	500	510	440	350	300	280
	5.5	125	250	440	500	530	560	560	570	490	390	330	310
	6.0	140	300	460	570	600	610	600	600	500	460	390	340
	6.5	150	350	530	630	650	690	680	700	580	540	400	370
	7.0	175	350	560	690	700	750	750	750	650	540	440	400

Table A2
Power matrix for AquaBuoy in kW with the rated power of 250 kW [79].

	T_p (s)												
H_{m0} (m)		**5.0**	**6.0**	**7.0**	**8.0**	**9.0**	**10.0**	**11.0**	**12.0**	**13.0**	**14.0**	**15.0**	**16.0**	**17.0**
	1.0	0	0	8	11	12	11	10	8	7	0	0	0	0
	1.5	0	13	17	25	27	26	23	19	15	12	12	12	7
	2.0	0	24	30	44	49	47	41	34	28	23	23	23	12
	2.5	0	37	47	69	77	73	64	54	43	36	36	36	19
	3.0	0	54	68	99	111	106	92	77	63	51	51	51	27
	3.5	0	0	93	135	152	144	126	105	86	70	70	70	38
	4.0	0	0	0	122	176	198	188	164	137	112	91	91	49
	4.5	0	0	0	223	250	239	208	173	142	115	115	115	62
	5.0	0	0	0	250	250	250	250	214	175	142	142	142	77
	5.5	0	0	0	250	250	250	250	250	211	172	172	172	92

Table A3
Power matrix for AWS (Archimedes WaveSwing) with a rated power of 2470 kW [80].

H_{m0} (m)	T_e (s) 5.0	5.5	6.0	6.5	7.0	7.5	8.0	8.5	9.0	9.5	10.0	10.5	11.0	11.5	12.0	12.5	13.0	13.5	14.0	14.5
0.5	0	0	0	0	0	0	0	0	0	0	0	0	0	0	0	0	0	0	0	0
1.0	2	7	13	19	26	34	41	48	58	68	81	93	105	118	131	144	153	163	183	203
1.5	4	15	28	41	56	72	85	99	121	143	173	203	226	248	266	285	309	334	357	380
2.0	8	26	49	73	100	127	150	172	210	247	292	337	366	395	418	442	482	523	543	563
2.5	15	43	78	113	159	205	234	263	320	376	438	499	531	563	603	643	675	708	741	774
3.0	25	61	111	161	227	293	339	386	453	521	600	680	722	765	827	888	897	906	945	984
3.5	35	92	155	218	305	391	454	517	605	694	772	851	913	975	1036	1096	1119	1141	1163	1185
4.0	35	114	194	273	380	486	572	659	776	894	961	1027	1103	1179	1227	1275	1316	1357	1365	1374
4.5	0	0	235	232	479	626	722	819	957	1096	1168	1240	1320	1401	1449	1497	1547	1598	1590	1583
5.0	0	0	280	400	592	784	899	1014	1144	1274	1380	1487	1569	1651	1691	1731	1785	1838	1807	1777
5.5	0	0	320	432	641	849	1033	1216	1331	1446	1568	1690	1778	1867	1919	1970	1977	1984	1994	2005
6.0	0	0	0	0	680	944	1155	1367	1495	1623	1759	1895	1936	2072	2137	2202	2205	2207	2226	2246
6.5	0	0	0	0	720	1123	1335	1547	1678	1809	1936	2116	2200	2284	2332	2380	2425	2470	2452	2434

Table A4
The power matrix for OEBuoy in kW with the rated power of 2880 kW [80].

H_{m0} (m)	T_p (s) 4.0	5.0	6.0	7.0	8.0	9.0	10.0	11.0	12.0	13.0	14.0	15.0	16.0
1.0	8	17	27	42	56	59	52	44	40	38	40	38	30
1.5	17	39	61	96	126	132	117	99	89	87	89	85	66
2.0	30	69	108	170	224	235	208	177	159	154	159	151	118
2.5	47	108	169	266	350	368	324	276	249	241	248	236	185
3.0	68	155	244	383	504	530	467	398	358	347	357	340	266
3.5	93	212	332	521	686	721	636	542	487	472	486	463	362
4.0	121	276	433	680	896	942	831	708	636	616	634	605	473
4.5	154	350	548	861	1130	1190	1050	896	805	780	803	765	599
5.0	190	432	677	1060	1400	1470	1300	1110	994	963	991	945	739
5.5	0	523	819	1290	1690	1780	1570	1340	1200	1170	1200	1140	894
6.0	0	622	975	1530	2020	2120	1870	1590	1430	1390	1430	1360	1060
6.5	0	730	1140	1800	2370	2490	2190	1870	1680	1630	1670	1600	1250
7.0	0	847	1330	2080	2750	2880	2540	2170	1950	1890	1940	1850	1450

Table A5
Power matrix for Pontoon in kW with the rated power of 3619 kW [80].

	T_p (s)													
H_{m0} *(m)*		**4.0**	**5.0**	**6.0**	**7.0**	**8.0**	**9.0**	**10.0**	**11.0**	**12.0**	**13.0**	**14.0**	**15.0**	**16.0**
	1.0	180	166	153	171	125	87	72	65	85	85	37	29	16
	1,5	223	195	157	148	261	192	223	139	155	155	74	67	46
	2.0	0	0	214	227	396	335	237	235	172	138	115	104	70
	2,5	0	0	0	440	598	514	379	342	204	169	142	128	95
	3.0	0	0	0	681	801	735	594	486	199	174	151	134	121
	3,5	0	0	0	904	1035	949	788	617	239	209	183	164	146
	4.0	0	0	0	1131	1269	1163	982	743	285	248	216	195	175
	4,5	0	0	0	1358	1488	1374	1187	869	330	287	250	225	201
	5.0	0	0	0	1585	1712	1585	1392	988	380	334	285	263	226
	5,5	0	0	0	1812	1937	1798	2138	1107	429	381	323	301	261
	6.0	0	0	0	2040	2162	2010	2884	1234	439	416	361	336	295
	6,5	0	0	0	2267	2386	2221	3143	1360	449	450	406	372	329
	7.0	0	0	0	2494	2611	2433	3619	1483	506	464	451	408	363

Table A6
Power matrix for Langlee (Floating 3 Body Oscillating Flap) in kW with the rated power of 1665 kW [81].

	T_p (s)													
H_{m0} *(m)*		**4.0**	**5.0**	**6.0**	**7.0**	**8.0**	**9.0**	**10.0**	**11.0**	**12.0**	**13.0**	**14.0**	**15.0**	**16.0**
	1.0	19	29	47	57	52	37	29	20	17	13	9	7	7
	1,5	42	63	92	111	109	65	56	38	29	22	19	13	11
	2.0	66	99	151	201	165	105	85	59	52	41	23	24	19
	2,5	0	160	242	262	226	166	118	83	70	57	39	29	26
	3.0	0	213	319	372	327	211	152	116	94	75	66	45	42
	3,5	0	0	436	503	408	293	203	148	115	93	75	58	44
	4.0	0	0	554	540	521	355	261	192	144	123	84	81	56
	4,5	0	0	645	746	587	379	302	236	190	154	106	90	74
	5.0	0	0	796	926	695	486	341	287	211	168	136	111	94
	5,5	0	0	0	955	808	603	430	343	231	201	150	120	97
	6.0	0	0	0	1161	957	642	481	329	289	212	172	146	111
	6,5	0	0	0	1476	1039	702	488	397	312	237	204	153	120
	7.0	0	0	0	1665	1197	821	612	466	385	252	223	181	146

Table A7
Power matrix for CETO in kW with the rated power of 260 kW [82].

	T_e (s)												
H_{m0} *(m)*		**4.0**	**5.0**	**6.0**	**7.0**	**8.0**	**9.0**	**10.0**	**11.0**	**12.0**	**13.0**	**14.0**	**15.0**
	1.0	0	0	0	0	0	0	0	0	0	0	0	0
	1.5	1	8	15	15	2	2	0	0	0	0	0	0
	2.0	0	29	34	29	19	13	5	0	0	0	0	0
	2.5	0	47	49	44	41	31	20	25	7	2	0	2
	3.0	0	51	60	54	51	43	36	20	15	7	1	3
	3.5	0	0	92	74	54	51	43	31	25	15	14	10
	4.0	0	0	110	116	91	53	51	43	35	25	18	23
	4.5	0	0	147	147	102	87	58	51	46	35	29	28
	5.0	0	0	178	193	138	111	70	52	52	44	35	29
	5.5	0	0	0	227	183	130	78	63	50	47	37	37
	6.0	0	0	0	252	225	168	122	82	68	52	43	49
	6.5	0	0	0	260	240	194	157	109	91	69	50	53

Table A8
Power matrix for Oyster 2 -Bottom Fixed Oscillating Flap Buoy (B-OF) in kW with the rated power of 3332 kW [83].

	T_e (s)												
H_{m0} (m)	**4.0**	**5.0**	**6.0**	**7.0**	**8.0**	**9.0**	**10.0**	**11.0**	**12.0**	**13.0**	**14.0**	**15.0**	**16.0**
1.0	27	39	57	76	87	104	109	100	101	98	94	94	87
1.5	63	92	126	188	201	213	201	239	207	198	183	150	154
2.0	75	180	233	301	380	408	383	399	329	365	319	265	259
2.5	0	254	378	467	568	623	618	601	519	523	481	390	428
3.0	0	368	503	693	799	824	876	792	759	704	546	579	554
3.5	0	0	655	934	1032	1085	1241	1075	973	925	862	747	688
4.0	0	0	843	1093	1352	1427	1430	1390	1158	1224	1139	1138	863
4.5	0	0	1219	1408	1844	1877	1807	1841	1862	1562	1404	1370	1191
5.0	0	0	1247	1871	1965	1962	2000	2000	1833	1798	1814	1459	1442
5.5	0	0	0	1979	2339	2308	2115	2389	2120	2013	1940	1518	1587
6.0	0	0	0	2406	2713	2776	2344	2705	2451	2396	2182	2414	2133
6.5	0	0	0	2778	3044	3001	2989	3211	2986	2896	2716	2455	2309
7.0	0	0	0	2871	3119	3131	3127	3176	3332	2877	2925	2676	2658

Table A9
Power matrix for Oyster in kW with the rated power of 290 kW [84].

	T_e (s)								
H_{m0} (m)	**5.0**	**6.0**	**7.0**	**8.0**	**9.0**	**10.0**	**11.0**	**12.0**	**13.0**
0.5	0	0	0	0	0	0	1	3	3
1.0	20	30	38	42	44	44	45	47	45
1.5	80	85	92	97	102	103	104	100	104
2.0	140	147	152	158	155	155	160	161	156
2.5	192	197	208	202	203	209	211	201	204
3.0	241	237	237	241	243	230	236	231	235
3.5	0	271	272	269	268	267	270	260	260
4.0	0	291	290	290	280	287	276	278	277
4.5	0	291	290	290	280	287	276	278	277
5.0	0	0	290	290	280	287	276	278	277
5.5	0	0	290	290	280	287	276	278	277
6.0	0	0	290	290	280	287	276	278	277

Table A10
Power matrix for SeaBased AB in kW with the rated power of 15 kW [85].

	T_p (s)												
H_{m0} (m)	**4.0**	**5.0**	**6.0**	**7.0**	**8.0**	**9.0**	**10.0**	**11.0**	**12.0**	**13.0**	**14.0**	**15.0**	**16.0**
1.0	1.2	1.3	1.2	1.2	1.1	1.0	0.9	0.8	0.7	0.7	0.7	0.6	0.7
1.5	2.6	2.5	2.3	2.2	2.3	2.0	1.9	1.7	1.4	1.5	1.2	1.2	1.2
2.0	4.4	4.0	3.7	3.6	3.5	3.1	2.8	2.5	2.3	2.2	2.0	1.8	1.7
2.5	0.0	6.0	5.2	4.5	4.6	4.3	3.9	3.6	3.0	2.8	2.5	2.7	2.6
3.0	0.0	7.4	6.7	6.2	5.7	5.4	4.7	4.1	4.1	3.7	3.3	3.3	3.2
3.5	0.0	0.0	8.4	7.3	6.9	5.8	5.4	4.9	4.4	4.2	3.7	3.4	3.6
4.0	0.0	0.0	8.9	8.6	7.6	6.8	6.2	5.6	5.0	4.6	4.5	4.3	3.6
4.5	0.0	0.0	10.6	9.5	8.7	7.6	7.0	6.1	5.9	5.4	5.1	5.0	4.7
5.0	0.0	0.0	12.2	10.8	9.8	8.6	7.3	7.2	6.3	5.9	5.7	5.4	5.0
5.5	0.0	0.0	0.0	11.1	10.1	8.9	8.1	7.5	6.8	6.4	6.1	5.5	5.8
6.0	0.0	0.0	0.0	13.1	11.3	10.1	9.1	8.3	7.5	6.7	6.9	6.4	5.8
6.5	0.0	0.0	0.0	13.5	11.6	10.4	9.8	9.0	7.6	7.3	7.5	6.2	6.4
7.0	0.0	0.0	0.0	15.0	12.9	10.9	10.0	8.8	8.6	8.2	7.6	7.3	6.8

Table A11
Power matrix for SSG (Sea Slot-cone Generator) in kW with the rated power of 20000 kW [86].

H_{m0} (m)	T_e (s)	5.0	5.5	6.0	6.5	7.0	7.5	8.0	8.5	9.0	9.5	10.0	10.5	11.0	11.5
	0.5	99	109	119	129	139	149	159	169	179	189	198	208	218	228
	1.0	397	437	476	516	556	595	635	675	715	754	794	833	873	913
	1.5	893	982	1072	1161	1250	1340	1429	1518	1608	1697	1786	1875	1965	2054
	2.0	1588	1746	1905	2064	2223	2381	2540	2699	2858	3016	3175	3334	3493	3651
	2.5	2481	2729	2977	3225	3473	3721	3969	4217	4465	4713	4961	5209	5457	5705
	3.0	3572	3929	4287	4644	5001	5358	5715	6073	6430	6787	7144	7501	7859	8216
	3.5	4862	5348	5834	6321	6807	7203	7779	8265	9751	9238	9724	10210	10695	11183
	4.0	6350	6985	7620	8256	8891	9526	10161	10796	11431	12066	12701	13336	13971	14606
	4.5	8037	8841	9645	10448	11252	12056	12860	13663	14467	15271	16074	16878	17682	18486
	5.0	9923	10915	11907	12899	13892	14884	15876	16868	17860	18853	19845	20000	20000	20000
	5.5	12006	13207	14407	15608	16809	18009	19210	20000	20000	20000	20000	20000	20000	20000
	6.0	14288	15717	17146	18575	20000	20000	20000	20000	20000	20000	20000	20000	20000	20000
	6.5	16769	18446	20000	20000	20000	20000	20000	20000	20000	20000	20000	20000	20000	20000
	7.0	19448	20000	20000	20000	20000	20000	20000	20000	20000	20000	20000	20000	20000	20000
	7.5	20000	20000	20000	20000	20000	20000	20000	20000	20000	20000	20000	20000	20000	20000
	8.0	20000	20000	20000	20000	20000	20000	20000	20000	20000	20000	20000	20000	20000	20000

Table A12
Power matrix for Bottom Fixed Heave Buoy array in kW with the rated power of 2192 kW [81].

H_{m0} (m)	T_z (s)	3.0	4.0	5.0	6.0	7.0	8.0	9.0	10.0	11.0	12.0	13.0	14.0	15.0	16.0
	1.0	0	49	73	85	86	83	78	72	67	63	59	46	42	37
	1.5	54	136	193	205	196	182	167	153	142	132	123	107	94	80
	2.0	106	265	347	347	322	294	265	244	224	207	193	185	180	153
	2.5	175	429	522	499	457	412	372	337	337	288	267	225	236	228
	3.0	262	600	653	641	602	557	555	460	471	451	445	437	381	325
	3.5	0	0	0	900	848	785	717	662	656	557	551	571	580	478
	4.0	0	0	0	1123	1098	1030	984	825	857	821	830	735	635	652
	4.5	0	0	0	1339	1339	1202	1181	1050	1140	1012	948	863	845	828
	5.0	0	0	0	1689	1518	1403	1318	1248	1348	1115	1176	925	890	982
	5.5	0	0	0	0	1943	1749	1517	1477	1374	1395	1376	1289	1212	1117
	6.0	0	0	0	0	2192	2144	1618	1789	1586	1634	1783	1585	1346	1313

Table A13
The power matrix for Oceantec in kW with the rated power of 500 kW [87].

H_{m0} (m) \ T_p (s)	6.0	7.0	8.0	9.0	10.0	11.0	12.0	13.0	14.0	15.0	16.0	17.0	18.0
1.0	85	87	59	39	25	16	10	7	5	3	2	2	1
1.5	191	196	133	89	57	36	23	15	10	7	5	3	3
2.0	339	348	234	158	101	64	41	27	18	12	9	6	4
2.5	500	500	364	245	158	101	65	42	28	19	13	10	7
3.0	500	500	500	337	228	145	93	61	41	28	19	14	10
3.5	500	500	500	420	309	196	127	83	55	38	26	19	13
4.0	500	500	500	500	401	258	166	109	72	49	34	24	18
4.5	500	500	500	500	500	326	210	138	92	62	43	31	22
5.0	500	500	500	500	500	383	259	170	113	77	54	38	27
5.5	500	500	500	500	500	389	308	205	137	93	65	46	33

Table A14
Power matrix for WaveStar in kW with the rated power of 600 kW [88].

H_{m0} (m) \ T_e (s)	3.0	4.0	5.0	6.0	7.0	8.0	9.0	10.0	11.0	12.0	13.0
0.5	0	0	0	0	0	0	0	0	0	0	0
1.0	0	49	73	85	86	83	78	82	67	63	59
1.5	54	136	193	205	196	182	187	153	142	132	123
2.0	106	265	347	347	322	294	265	244	224	207	193
2.5	175	429	522	499	457	412	372	337	312	288	267
3.0	262	600	600	600	600	540	484	442	399	367	340

Table A15
Power matrix for P*WEC* in kW with the rated power of 479 kW [89].

H_{m0} (m) \ T_p (s)	4.0	6.0	8.0	10.0	12.0	14.0	16.0	18.0
0.5	2.8	5.4	6.8	10.7	6.8	4.4	3.1	2.3
1.5	0.0	48.0	54.7	69.0	61.8	40.5	28.8	21.3
2.5	0.0	130.9	135.9	152.7	144.8	116.7	83.5	63.2
3.5	0.0	0.0	230.9	241.6	236.6	214.9	155.6	123.4
4.5	0.0	0.0	0.0	324.0	321.4	287.6	240.2	189.4
5.5	0.0	0.0	0.0	389.4	387.9	366.7	314.0	252.3
6.5	0.0	0.0	0.0	0.0	444.9	429.2	371.1	306.7
7.5	0.0	0.0	0.0	0.0	0.0	479.1	423.4	353.6

Table A16
Power matrix for Pelamis in kW with the rated power of 750 kW [90].

H_{m0} (m) \ T_e (s)	5.0	5.5	6.0	6.5	7.0	7.5	8.0	8.5	9.0	9.5	10.0	10.5	11.0	11.5	12.0	12.5	13.0
0.5	0	0	0	0	0	0	0	0	0	0	0	0	0	0	0	0	0
1.0	0	22	29	34	37	38	38	37	35	32	29	26	23	21	0	0	0
1.5	32	50	65	76	83	86	86	83	78	72	65	59	53	47	42	37	33
2.0	57	88	115	136	148	153	152	147	138	127	116	104	93	83	74	66	59
2.5	89	138	180	212	231	238	238	230	216	199	181	163	146	130	116	103	92
3.0	129	198	260	305	332	340	332	315	292	266	240	219	210	188	167	149	132
3.5	0	270	354	415	438	440	424	404	377	362	326	292	260	230	215	202	180
4.0	0	0	462	502	540	546	530	499	475	429	384	366	339	301	267	237	213
4.5	0	0	544	635	642	648	628	590	562	528	473	432	382	356	338	300	266
5.0	0	0	0	739	726	731	707	687	670	607	557	521	472	417	369	348	328
5.5	0	0	0	750	750	750	750	750	737	667	658	586	530	496	446	395	355
6.0	0	0	0	0	750	750	750	750	750	750	711	633	619	558	512	470	415
6.5	0	0	0	0	750	750	750	750	750	750	750	743	658	621	579	512	481
7.0	0	0	0	0	0	750	750	750	750	750	750	750	750	676	613	584	525
7.5	0	0	0	0	0	0	750	750	750	750	750	750	750	750	686	622	593
8.0	0	0	0	0	0	0	0	750	750	750	750	750	750	750	750	750	690

Table A17
Power matrix for WaveBob (Floating 2 Body Heaving Converter, F-2HB) in kW with the rated power of 1000 kW [80].

H_{m0} (m) \ T_p (s)	4.0	5.0	6.0	7.0	8.0	9.0	10.0	11.0	12.0	13.0	14.0	15.0	16.0
1.0	6	11	19	25	30	44	50	53	44	34	22	20	17
1.5	13	25	43	55	68	90	102	92	91	66	65	45	37
2.0	24	45	65	100	121	153	175	151	122	126	87	61	58
2.5	0	65	104	141	191	179	243	255	190	181	135	99	83
3.0	0	96	137	205	244	357	293	353	260	248	184	137	120
3.5	0	0	192	254	291	431	385	424	314	285	239	222	172
4.0	0	0	256	366	403	551	536	531	473	420	289	268	179
4.5	0	0	327	418	574	678	708	665	509	415	386	244	249
5.0	0	0	358	514	658	824	828	618	638	512	452	384	333
5.5	0	0	0	610	774	880	936	905	805	603	456	397	311
6.0	0	0	0	711	952	974	1000	838	886	648	501	503	396
6.5	0	0	0	788	1000	1000	1000	979	1000	727	577	435	424
7.0	0	0	0	781	1000	1000	1000	1000	1000	959	748	574	472

Table A18
Power matrix for WaveDragon in kW with the rated power of 7000 kW [86].

H_{m0} (m) \ T_e (s)	5.0	6.0	7.0	8.0	9.0	10.0	11.0	12.0	13.0	14.0	15.0	16.0	17.0
1.0	160	250	360	360	360	360	360	360	320	280	250	220	180
2.0	640	700	840	900	1190	1190	1190	1190	1070	950	830	710	590
3.0	0	1450	1610	1750	2000	2620	2620	2620	2360	2100	1840	1570	1310
4.0	0	0	2840	3220	3710	4200	5320	5320	4430	3930	3440	2950	2460
5.0	0	0	0	4610	5320	6020	7000	7000	6790	6090	5250	3950	3300
6.0	0	0	0	0	6720	7000	7000	7000	7000	7000	6860	5110	4200
7.0	0	0	0	0	0	7000	7000	7000	7000	7000	7000	6650	5740

Appendix B

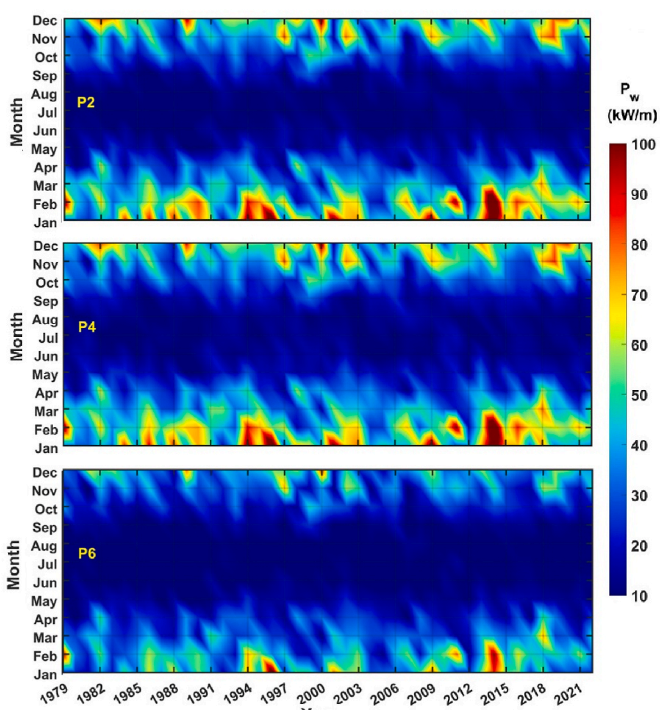

Fig. B1. Mean monthly wave energy flux variation across 44 years in three representative locations in the center of the concession zones designated by the Portuguese government labeled as P2, P4 and P6.

Appendix C

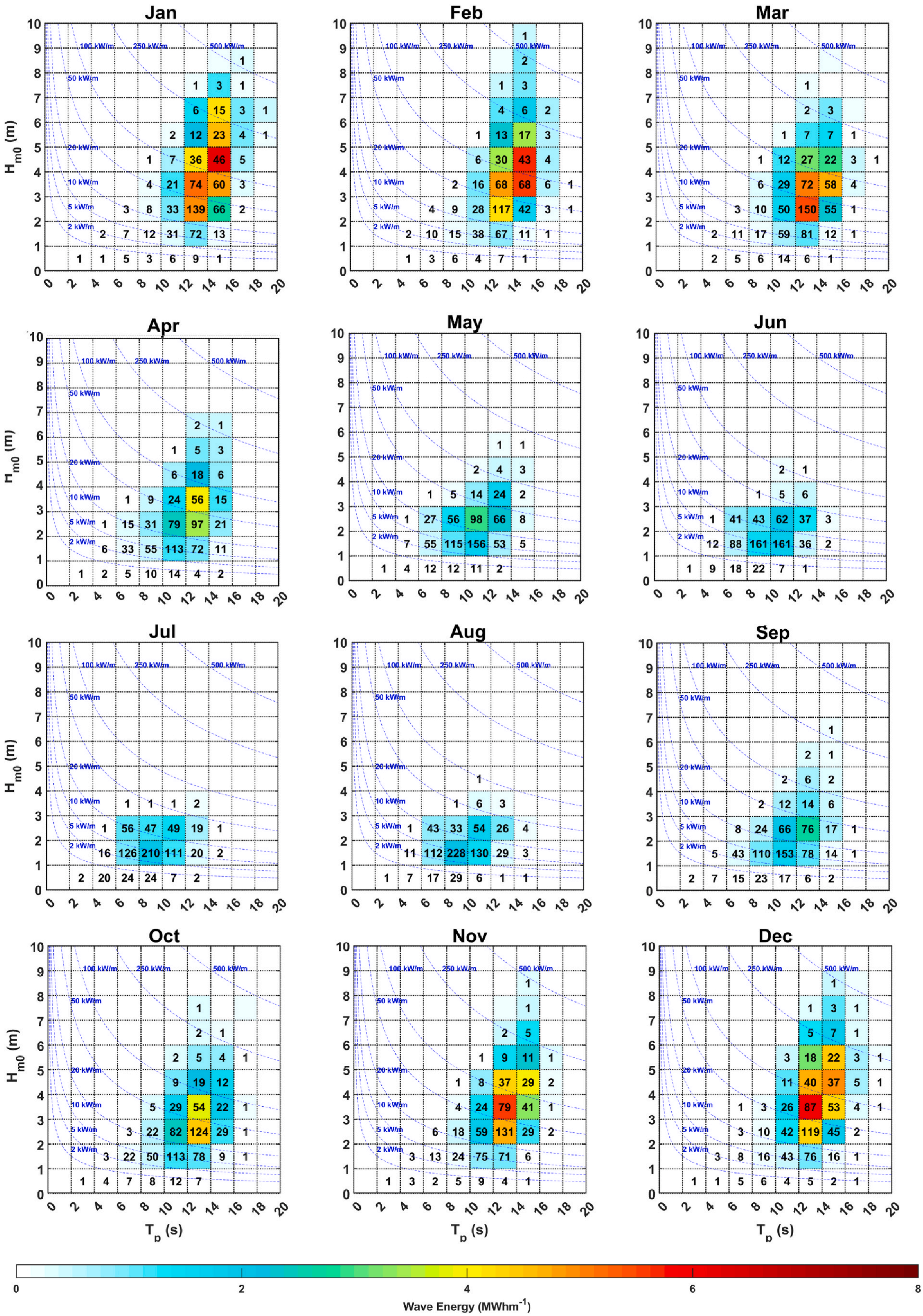

Fig. C1. Monthly scatter diagrams of the wave resources at P1 representative location in P1 concession zone designated by the Portuguese government.

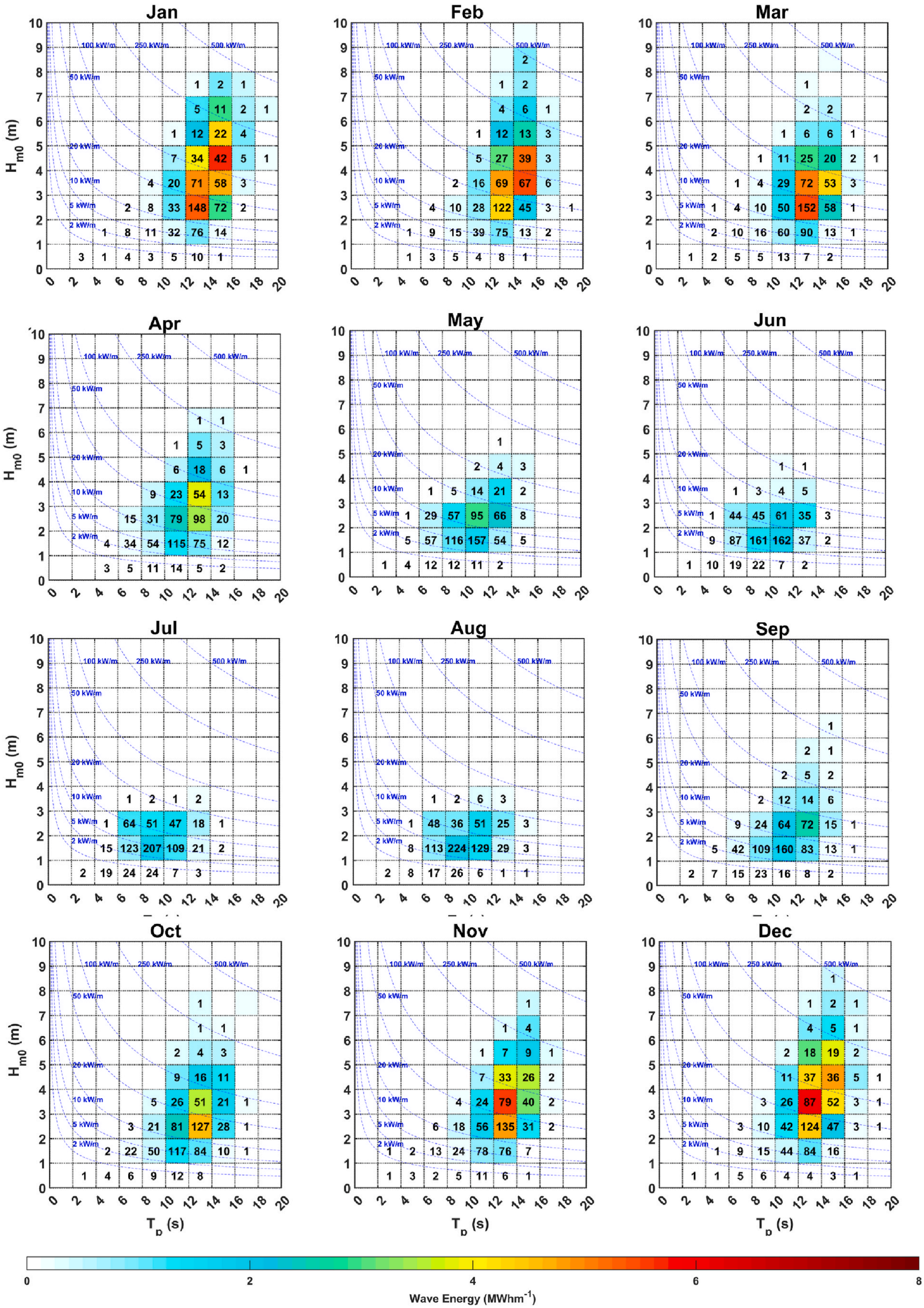

Fig. C2. Monthly scatter diagrams of the wave resources at P2 representative location in P2 concession zone designated by the Portuguese government.

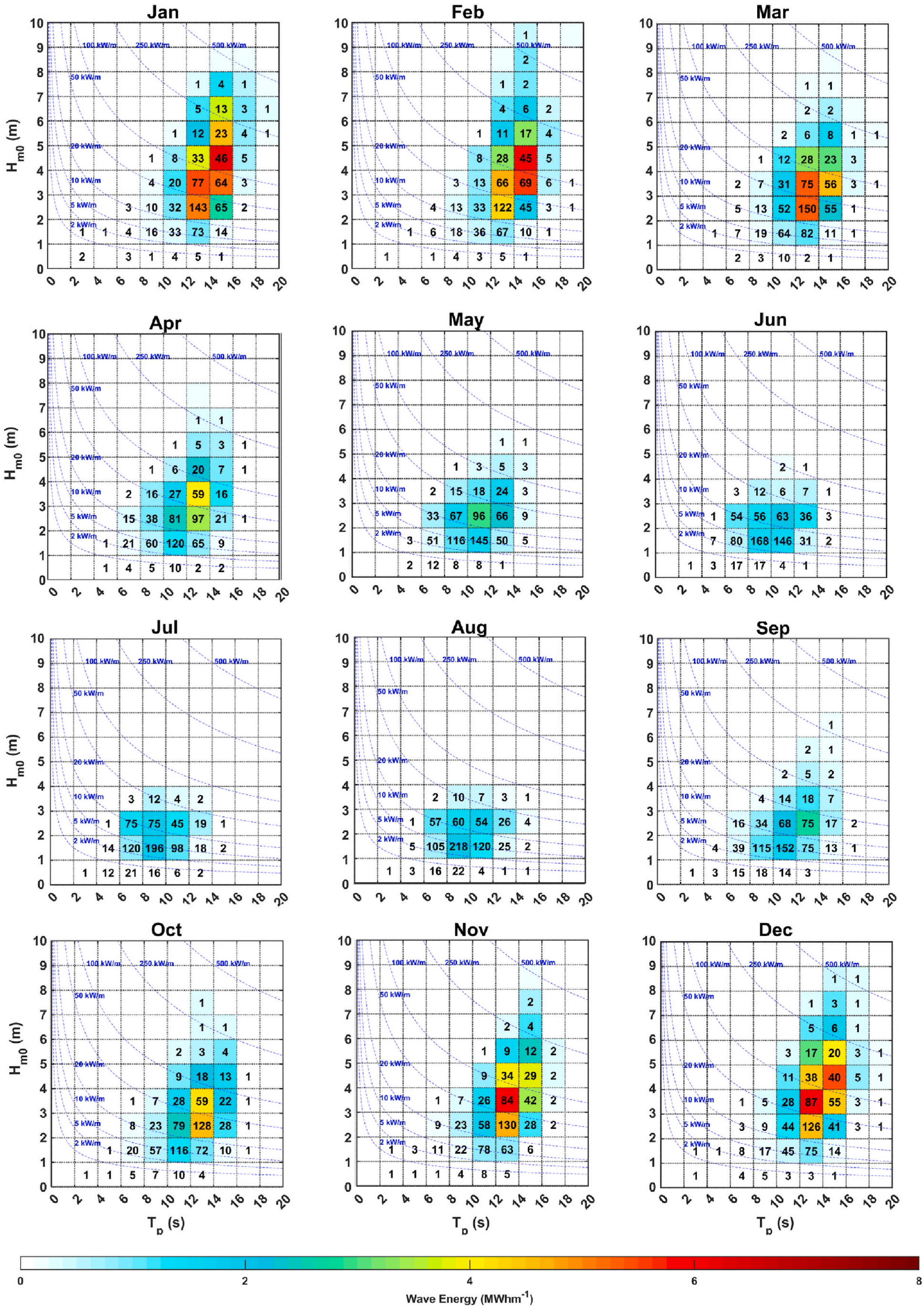

Fig. C3. Monthly scatter diagrams of the wave resources at P3 representative location in P3 concession zone designated by the Portuguese government.

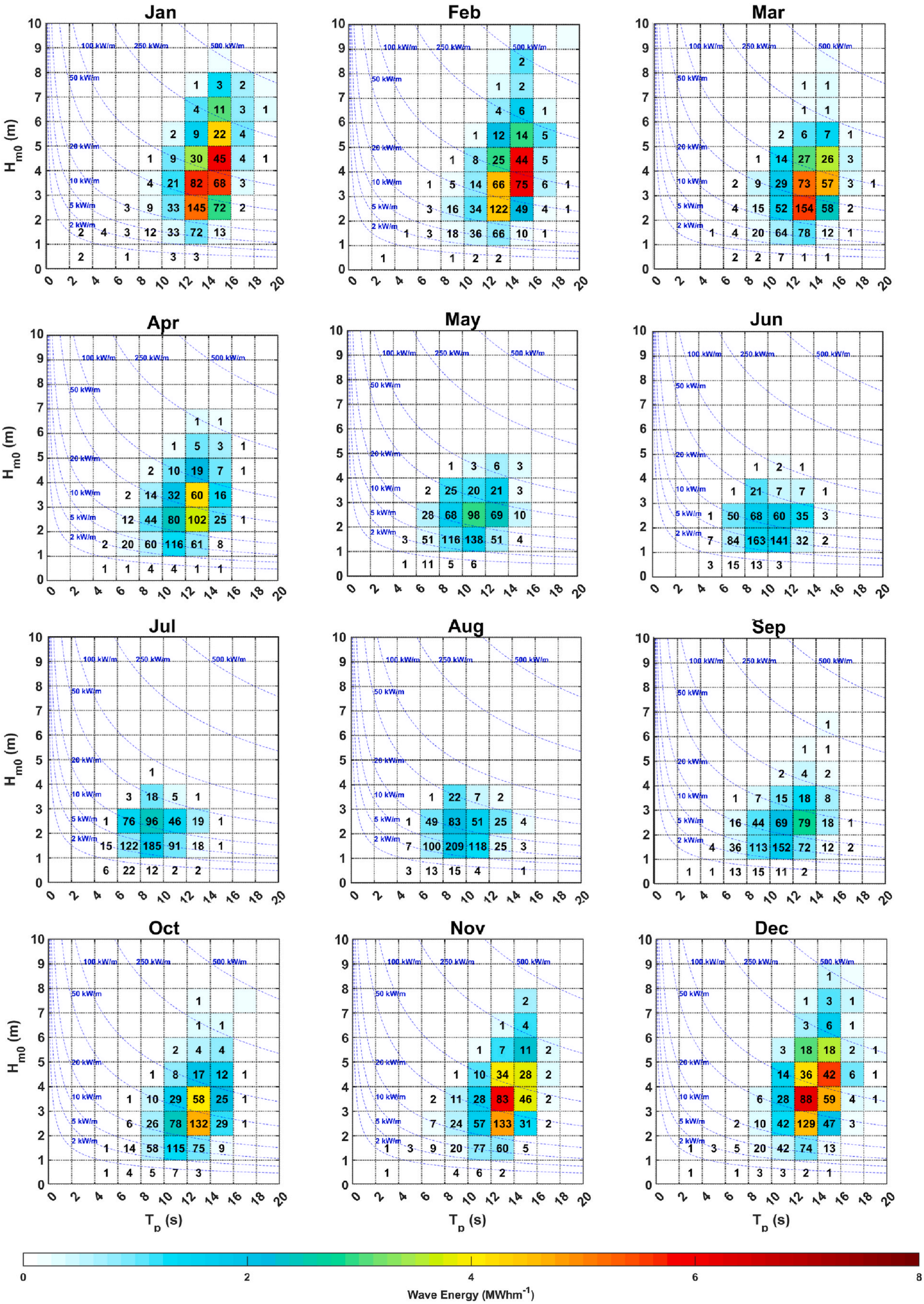

Fig. C4. Monthly scatter diagrams of the wave resources at P4 representative location in P4 concession zone designated by the Portuguese government.

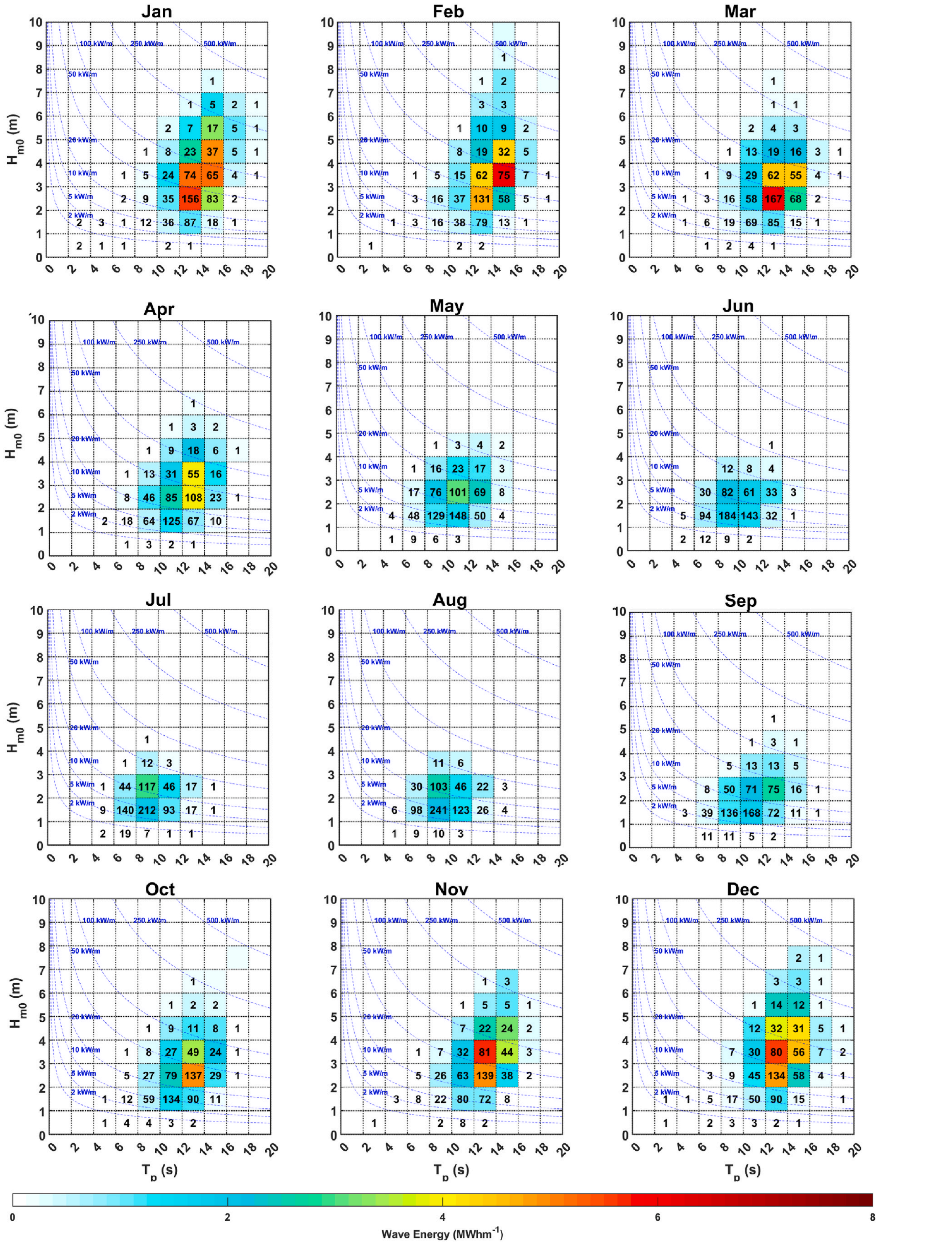

Fig. C5. Monthly scatter diagrams of the wave resources at P5 representative location in P5 concession zone designated by the Portuguese government.

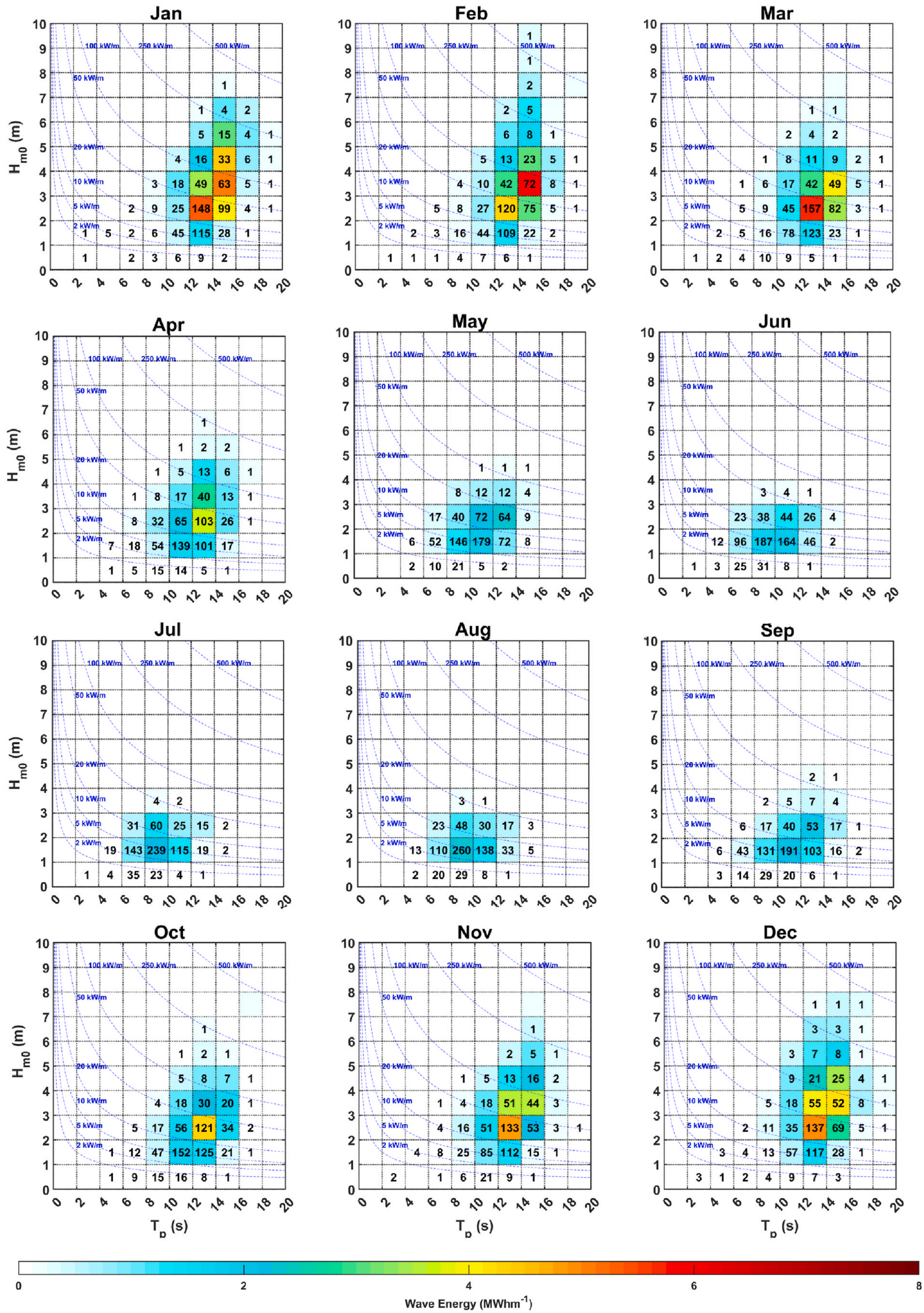

Fig. C6. Monthly scatter diagrams of the wave resources at P6 representative location in P6 concession zone designated by the Portuguese government.

Appendix D

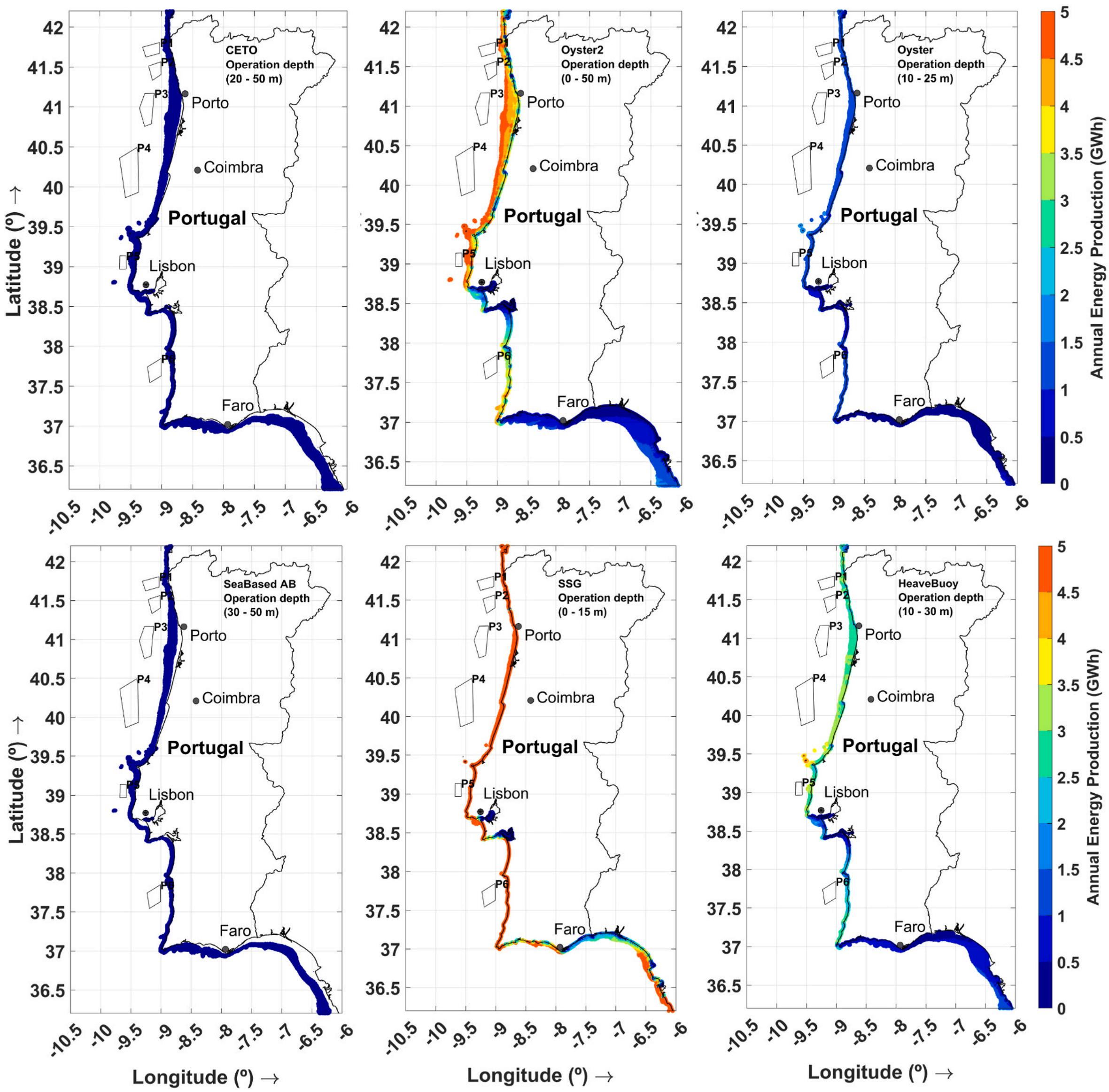

Fig. D1. Spatial distributions of mean annual energy production (*AEP*) for CETO, Oyster 2, Oyster SeaBased AB, SSG and Bottom Fixed HeaveBuoy *WECs* in their operation depth range.

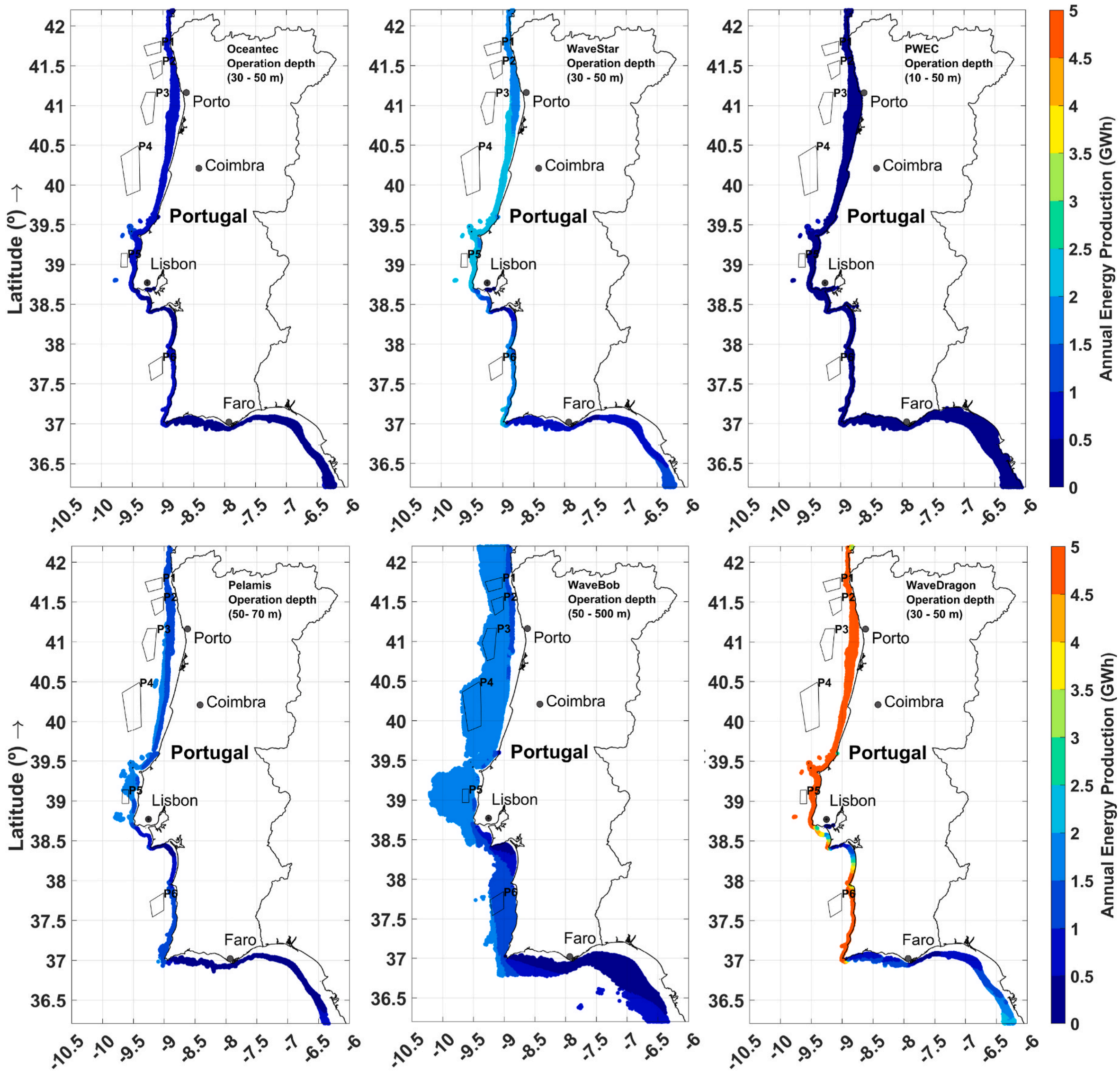

Fig. D2. Spatial distributions of mean annual energy production (*AEP*) for Oceantec, WaveStar, PWEC, Pelamis, WaveBob and WaveDragon WECs in their operation depth range.

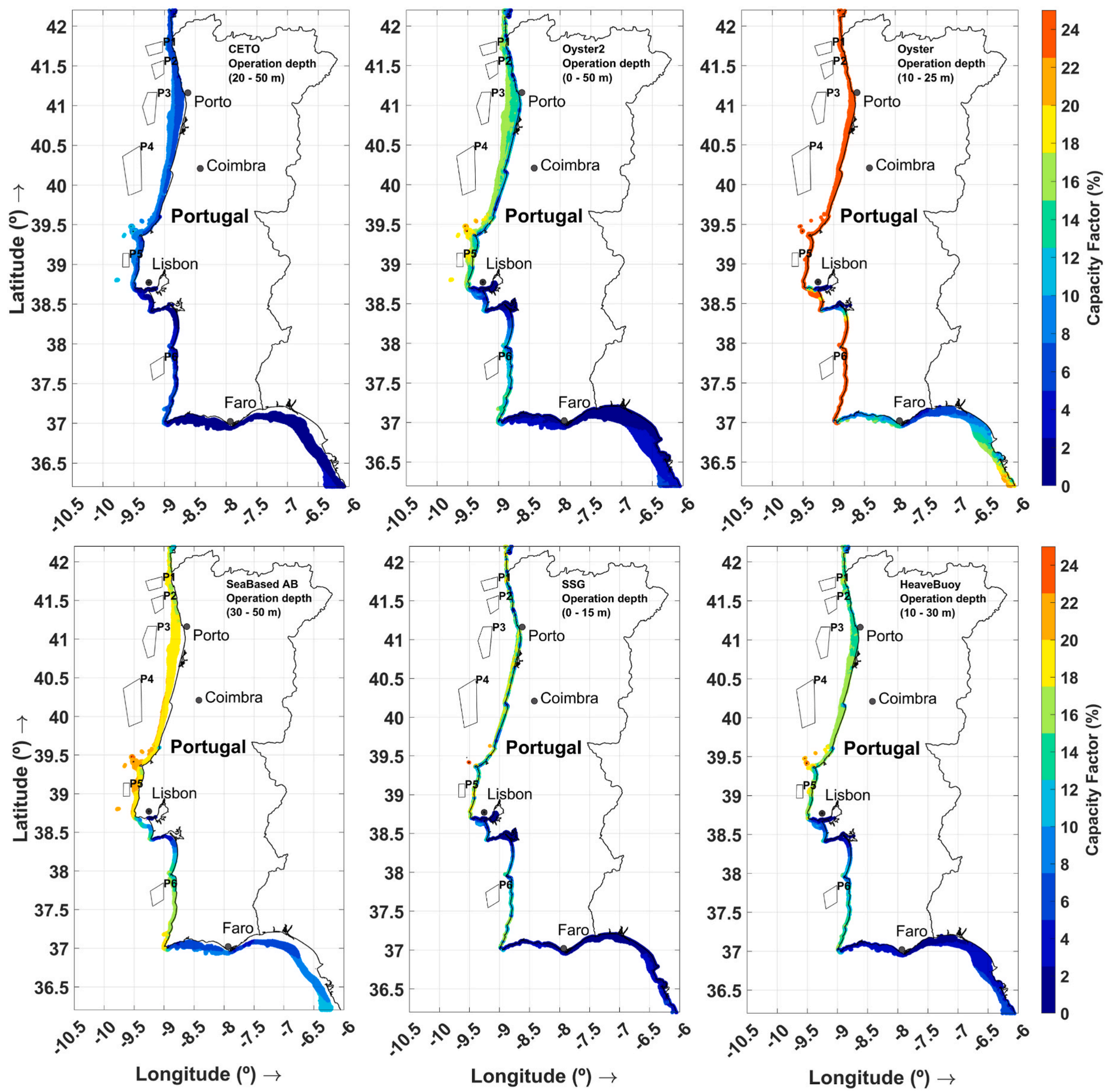

Fig. D3. Spatial distributions of capacity factor (c_f) for CETO, Oyster 2, Oyster SeaBased AB, SSG and Bottom Fixed HeaveBuoy WECs in their operation depth range.

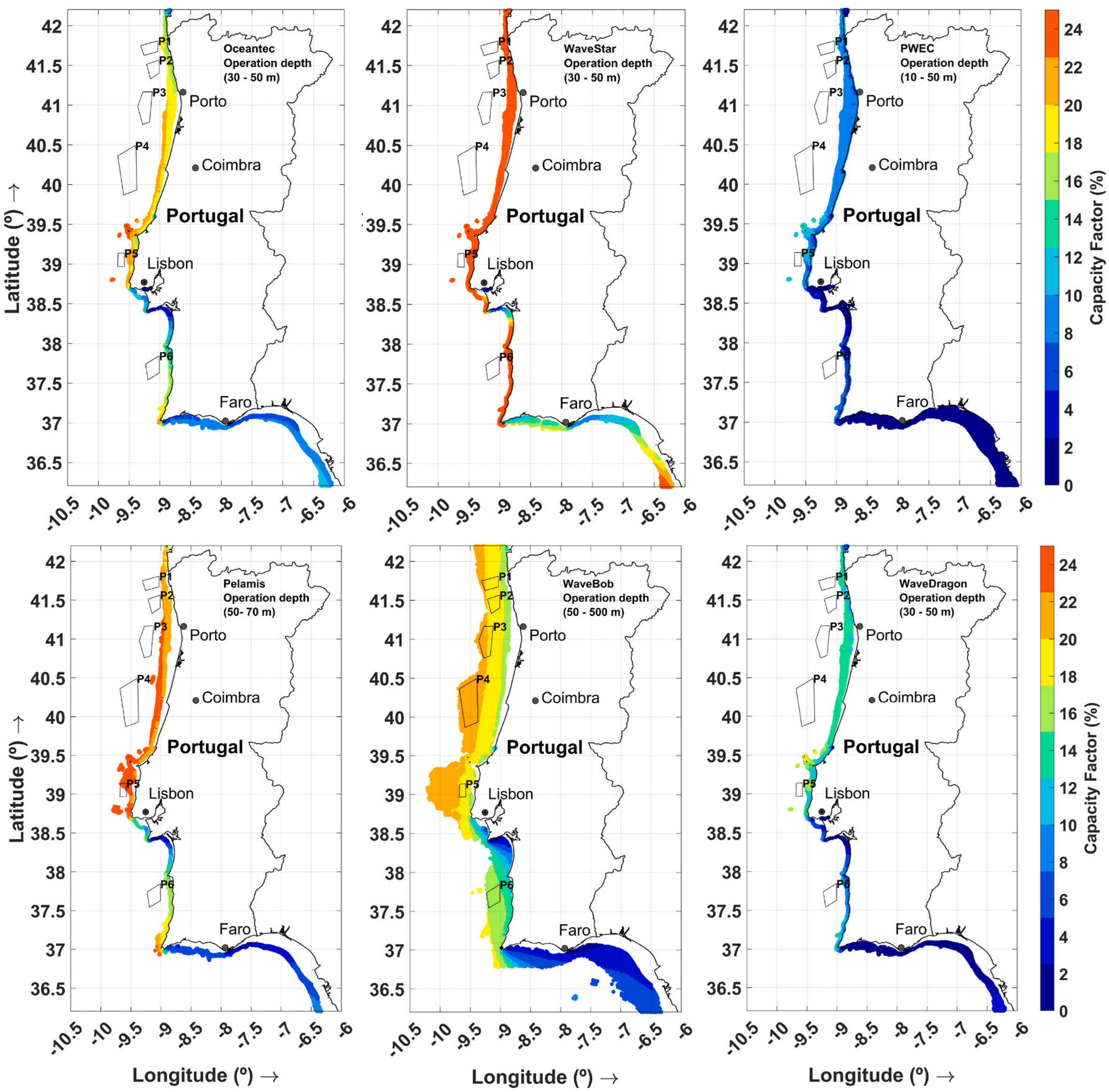

Fig. D4. Spatial distributions of capacity factor (c_f) for Oceantec, WaveStar, PWEC, Pelamis, WaveBob and WaveDragon *WEC*s in their operation depth range.

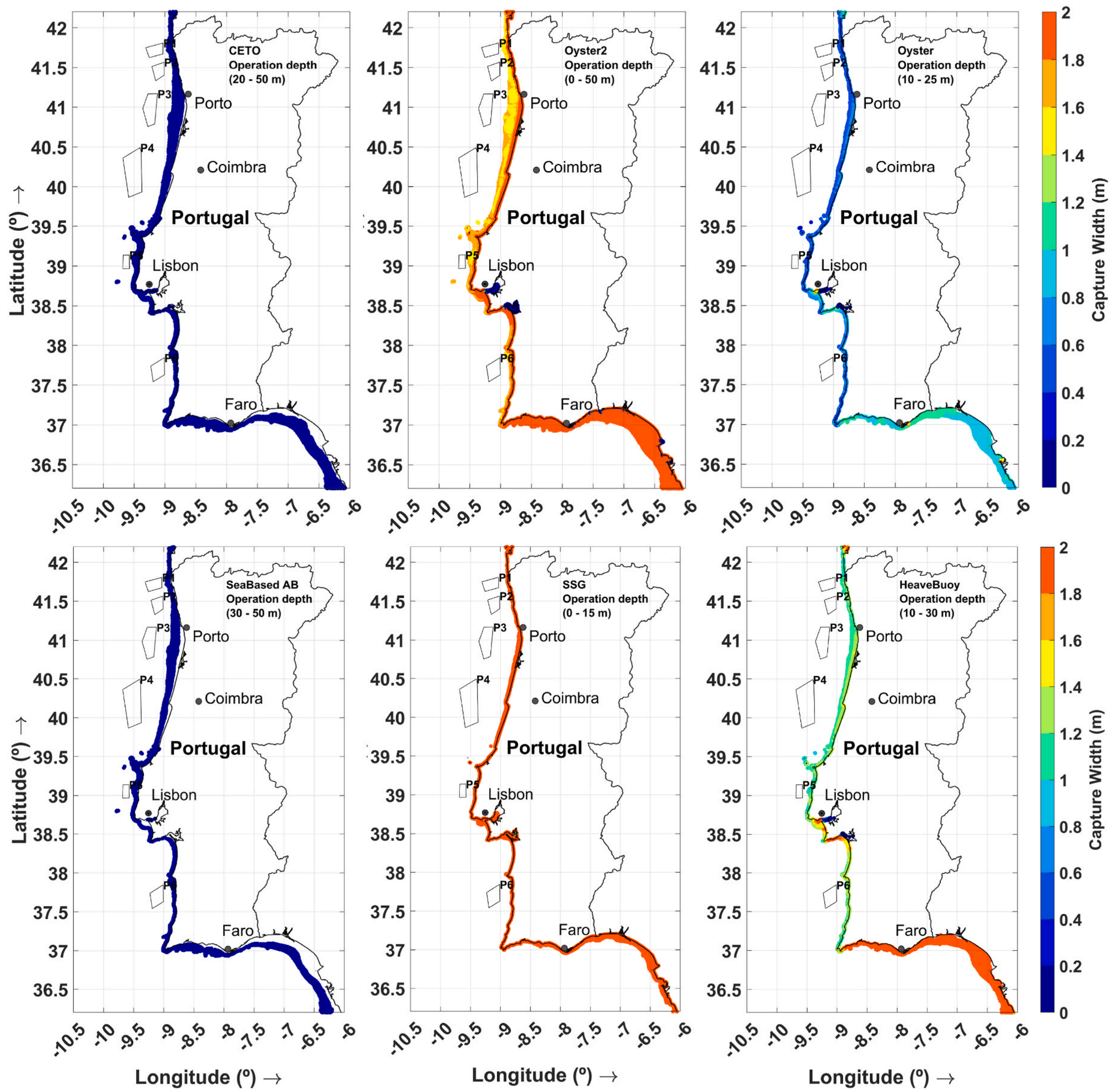

Fig. D5. Spatial distributions of capture width (c_w) for CETO, Oyster 2, Oyster SeaBased AB, SSG and Bottom Fixed HeaveBuoy WECs in their operation depth range.

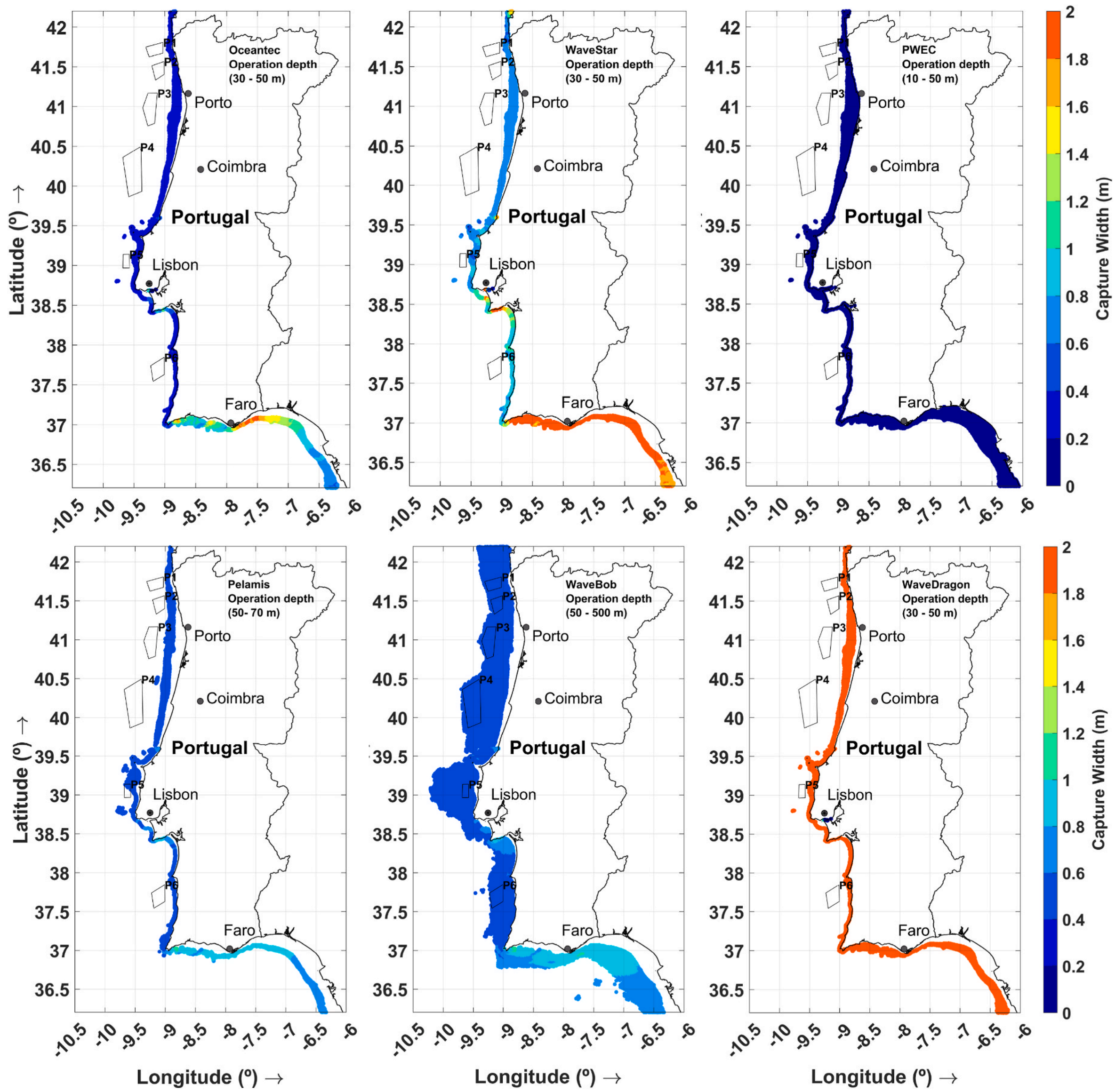

Fig. D6. Spatial distributions of capture width (c_w) for Oceantec, WaveStar, PWEC, Pelamis, WaveBob and WaveDragon *WECs* in their operation depth range.

References

[1] B. Bingölbali, A.G. Majidi, A. Akpınar, Inter- and intra-annual wave energy resource assessment in the south-western Black Sea coast, Renew. Energy 169 (2021) 809–819, https://doi.org/10.1016/J.RENENE.2021.01.057.

[2] A.G. Majidi, V. Ramos, G. Giannini, P. Rosa Santos, L. das Neves, F. Taveira-Pinto, The impact of climate change on the wave energy resource potential of the Atlantic Coast of Iberian Peninsula, Ocean. Eng. 284 (2023) 115451, https://doi.org/10.1016/J.OCEANENG.2023.115451.

[3] X. Zhang, H. Zhang, X. Zhou, Z. Sun, Recent advances in wave energy converters based on nonlinear stiffness mechanisms, Appl. Math. Mech. 43 (2022) 1081–1108, https://doi.org/10.1007/S10483-022-2864-6/METRICS.

[4] G. Lavidas, K. Blok, Shifting wave energy perceptions: the case for wave energy converter (WEC) feasibility at milder resources, Renew. Energy 170 (2021) 1143–1155, https://doi.org/10.1016/j.renene.2021.02.041.

[5] L. Wan, T. Moan, Z. Gao, W. Shi, A review on the technical development of combined wind and wave energy conversion systems, Energy 294 (2024) 130885, https://doi.org/10.1016/j.energy.2024.130885.

[6] T. Calheiros-Cabral, A.G. Majidi, V. Ramos, G. Giannini, P. Rosa-Santos, F. Taveira-Pinto, Development and assessment of a hybrid breakwater-integrated wave energy converter, Intern. Marine Energy J. 5 (2022) 281–291, https://doi.org/10.36688/imej.5.281-291.

[7] C. Guo, W. Sheng, D.G. De Silva, G. Aggidis, A review of the levelized cost of wave energy based on a techno-economic model, Energies 16 (2023) 2144, https://doi.org/10.3390/en16052144.

[8] H. Bouhrim, A. El Marjani, R. Nechad, I. Hajjout, Ocean wave energy conversion: a review, J. Mar. Sci. Eng. 12 (2024) 1922, https://doi.org/10.3390/jmse12111922.

[9] M. Corrales-Gonzalez, G. Lavidas, A. Lira-Loarca, G. Besio, Wave energy assessment and wave converter applicability at the Pacific coast of Central America, Front. Energy Res. 12 (2024), https://doi.org/10.3389/fenrg.2024.1454275.

[10] A. Trueworthy, B. DuPont, The wave energy converter design process: methods applied in industry and shortcomings of current practices, J. Mar. Sci. Eng. 8 (2020) 932, https://doi.org/10.3390/jmse8110932.

[11] N. Tom, K. Ruehl, A. Keester, D. Forbush, D. Ogden, J. Leon, S. Husain, J. Grasberger, M.B.R. Topper, Y.-H. Yu, New Developments and Capabilities within WEC-Sim, American Society of Mechanical Engineers Digital Collection, 2023, https://doi.org/10.1115/OMAE2023-105030.

[12] V.S. Neary, S. Ahn, B.E. Seng, M.N. Allahdadi, T. Wang, Z. Yang, R. He, Characterization of extreme wave conditions for wave energy converter design and project risk assessment, J. Mar. Sci. Eng. 8 (2020) 289, https://doi.org/10.3390/jmse8040289.

[13] A. Maria-Arenas, A.J. Garrido, E. Rusu, I. Garrido, Control strategies applied to wave energy converters: state of the art, Energies 12 (2019) 3115, https://doi.org/10.3390/en12163115.

[14] T. Aderinto, H. Li, Review on power performance and efficiency of wave energy converters, Energies 12 (2019) (2019) 4329, https://doi.org/10.3390/EN12224329. Vol. 12, Page 4329.

[15] P. Frigaard, A. Têtu, L. Margheritini, M.B. Kramer, Environmental conditions and test standards for the Danish wave energy center: 14th conference on sustainable development of energy, water and environment systems. Digital Proceedings of 14th Conference on Sustainable Development of Energy, Water and Environment Systems, 2019.

[16] D.E. Reeve, Y. Chen, S. Pan, V. Magar, D.J. Simmonds, A. Zacharioudaki, An investigation of the impacts of climate change on wave energy generation: the Wave Hub, Cornwall, UK, Renew. Energy 36 (2011) 2404–2413, https://doi.org/10.1016/J.RENENE.2011.02.020.

[17] M.J. Witt, E.V. Sheehan, S. Bearhop, A.C. Broderick, D.C. Conley, S.P. Cotterell, E. Crow, W.J. Grecian, C. Halsband, D.J. Hodgson, P. Hosegood, R. Inger, P. I. Miller, D.W. Sims, R.C. Thompson, K. Vanstaen, S.C. Votier, M.J. Attrill, B. J. Godley, Assessing wave energy effects on biodiversity: the Wave Hub experience, Phil. Trans. Math. Phys. Eng. Sci. 370 (2012) 502–529, https://doi.org/10.1098/rsta.2011.0265.

[18] H. Mouslim, A. Babarit, A. Clément, B. Borgarino, Development of the French wave energy test site SEM-REV, in: Proceedings of the 8th European Wave and Tidal Energy Conference, Laboratoire de Mécanique des Fluides Ecole Centrale de Nantes, Uppsala, Sweden, 2009, pp. 31–35.

[19] J.-B. Saulnier, I. Le Crom, Peakedness of Wave Systems Observed on the French Wave Energy Test Site (SEM-REV) Using a Spectral Partitioning Algorithm, American Society of Mechanical Engineers Digital Collection, 2013, https://doi.org/10.1115/OMAE2013-11470.

[20] B.G. Cahill, T. Lewis, Wave energy resource characterisation of the atlantic marine energy test site, Intern. J. Marine Energy 1 (2013) 3–15, https://doi.org/10.1016/j.ijome.2013.05.001.

[21] M. Chatzigiannakou, I. Temiz, M. Leijon, Offshore deployments of wave energy converters by seabased industry AB, J. Mar. Sci. Eng. 5 (2017) 15, https://doi.org/10.3390/jmse5020015.

[22] A. Palha, L. Mendes, C.J. Fortes, A. Brito-Melo, A. Sarmento, The impact of wave energy farms in the shoreline wave climate: Portuguese pilot zone case study using Pelamis energy wave devices, Renew. Energy 35 (2010) 62–77, https://doi.org/10.1016/j.renene.2009.05.025.

[23] J. Norris, I. Bryden, European marine energy centre: facilities and resources, Proce. Institu. Civil Eng.- Energy 160 (2007) 51–58, https://doi.org/10.1680/ener.2007.160.2.51.

[24] I.A. Cantero, L. Rodríguez-Méndez, N.V. Tubía, A.A. Iriarte, Integrated geological study in an offshore renewable energy test site: an example from the Basque contiental shelf, Bay of Biscay, Spain) (2024), https://doi.org/10.21203/rs.3.rs-4242811/v1.

[25] J. González, V. Monagas, E. Delory, J. Hernández, O. Llinás, A marine test site for ocean energy converters: oceanic Platform of the Canary Islands, in: OCEANS 2011 IEEE - Spain, 2011, pp. 1–6, https://doi.org/10.1109/Oceans-Spain.2011.6003471.

[26] J. González, V. Monagas, X. Remírez, A. Luque, J. Hernández, O. Llinás, PLOCAN. An offshore test site for ocean energy converters, in: OCEANS 2015 - Genova, 2015, pp. 1–4, https://doi.org/10.1109/OCEANS-Genova.2015.7271245.

[27] P. Frigaard, J.P. Kofoed, M.R. Rasmussen, Overtopping measurements on the wave dragon nissum bredning prototype, in: ISOPE International Ocean and Polar Engineering Conference, ISOPE-I). ISOPE, 2004, May.

[28] R. Atan, J. Goggins, S. Nash, Galway Bay – the 1/4 scale wave energy test site? A detailed wave energy resource assessment and investigation of scaling factors, Renew. Energy 119 (2018) 217–234, https://doi.org/10.1016/j.renene.2017.11.090.

[29] J. Walsh, I. Bashir, P.R. Thies, L. Johanning, Ph Blondel, Acoustic emission health monitoring of marine renewables: illustration with a wave energy converter in Falmouth Bay (UK), in: OCEANS 2015 - Genova, 2015, pp. 1–7, https://doi.org/10.1109/OCEANS-Genova.2015.7271455.

[30] B. Batten, D. Hellin, The Pacific Marine Energy Center - South Energy Test Site (PMEC-SETS), Oregon State Univ., Corvallis, OR (United States), 2018, https://doi.org/10.2172/1419795.

[31] M.C. Freeman, R. O'Neil, L. Garavelli, D. Hellin, J. Klure, Case study on the novel permitting and authorization of PacWave South, a US grid-connected wave energy test facility: development, challenges, and insights, Energy Pol. 168 (2022) 113141, https://doi.org/10.1016/j.enpol.2022.113141.

[32] L.A. Vega, Hawai'i national marine renewable energy center (HINMREC), in: OCEANS'11 MTS/IEEE, KONA, IEEE, Waikoloa, HI, 2011, pp. 1–4, https://doi.org/10.23919/OCEANS.2011.6107038.

[33] Chenhua Ni, Development of ocean energy test field in China, JSOE 5. https://doi.org/10.17265/2159-5879/2015.01.005, 2015.

[34] The public consultation-Porugal, Contributos para a consulta pública plano de afetação para as energias renováveis offshore resumo (Contributions to the public consultation plan for offshore renewable energy allocation summary), 2023.

[35] Directorate General for Energy and Geology-Portugal, Renewable Energy and Sustainability, Ocean Energy., https://www.dgeg.gov.pt/en/vertical-areas/energy/renewable-energy-andsustainability/ocean-energy/(accessed April 17, 2024).

[36] V. Ramos, M. López, F. Taveira-Pinto, P. Rosa-Santos, Influence of the wave climate seasonality on the performance of a wave energy converter: a case study, Energy 135 (2017) 303–316, https://doi.org/10.1016/J.ENERGY.2017.06.080.

[37] E.M. Blech, Developing a Cost Model for Combined Offshore Farms: the Advantages of Co-located Wind and Wave Energy, Master's Thesis, Universitat Politècnica de Catalunya, 2023.

[38] B. Guo, T. Wang, S. Jin, S. Duan, K. Yang, Y. Zhao, A review of point absorber wave energy converters, J. Mar. Sci. Eng. 10 (2022) 1534, https://doi.org/10.3390/jmse10101534.

[39] Eco Wave Power, Eco wave power secures 1MW installation and grid connection permit (Small-Production unit registration approval) for its planned pilot project in Portugal. https://www.ecowavepower.com/eco-wave-power-secures-1mw-installation-and-ridconnection-permit-small-production-unit-registration-approval-for-its-planned-pilot-project-inportugal/, 2021. (Accessed 26 April 2024).

[40] Energy Global, Portugal's plans for offshore renewables. https://www.energyglobal.com/special-reports/09082021/portugals-plans-for-offshorerenewables/, 2021. (Accessed 17 April 2024).

[41] C. Guedes Soares, A.R. Bento, M. Gonçalves, D. Silva, P. Martinho, Numerical evaluation of the wave energy resource along the Atlantic European coast, Comput. Geosci. 71 (2014) 37–49, https://doi.org/10.1016/j.cageo.2014.03.008.

[42] E. Rusu, Numerical modeling of the wave energy propagation in the iberian nearshore, Energies 11 (2018) 980, https://doi.org/10.3390/en11040980.

[43] E. Rusu, D. Silva, C. Guedes Soares, Efficiency assessment for different WEC types operating in the Portuguese coastal environment, in: Developments in Maritime Transportation and Exploitation of Sea Resources, 2014, pp. 961–969, https://doi.org/10.1201/b15813-120.

[44] V. Ramos, M. López, F. Taveira-Pinto, P. Rosa-Santos, Performance assessment of the CECO wave energy converter: water depth influence, Renew. Energy 117 (2018) 341–356, https://doi.org/10.1016/J.RENENE.2017.10.064.

[45] M. López, V. Ramos, P. Rosa-Santos, F. Taveira-Pinto, Effects of the PTO inclination on the performance of the CECO wave energy converter, Mar. Struct. 61 (2018) 452–466, https://doi.org/10.1016/j.marstruc.2018.06.016.

[46] A.S. Ribeiro, M. deCastro, L. Rusu, M. Bernardino, J.M. Dias, M. Gomez-Gesteira, Evaluating the future efficiency of wave energy converters along the NW coast of the iberian peninsula, Energies 13 (2020) 3563, https://doi.org/10.3390/en13143563.

[47] A.G. Majidi, V. Ramos, K. Amarouche, P. Rosa Santos, L. das Neves, F. Taveira-Pinto, Assessing the impact of wave model calibration in the uncertainty of wave energy estimation, Renew. Energy (2023), https://doi.org/10.1016/J.RENENE.2023.05.049.

[48] A.G. Majidi, V. Ramos, T. Calheiros-Cabral, L. das Neves, P. Rosa-Santos, F. Taveira-Pinto, Integrated assessment of offshore wind and wave power resources in mainland Portugal. https://doi.org/10.2139/ssrn.4834256, 2024.

[49] SWAN Team, SWAN User Manual—SWAN Cycle III Version 41.31 A, Delft University of Technology, Delft, 2020.

[50] T. Iec, 62600-101; Marine Energy–Wave, Tidal and Other Water Current Converters–Part 101: Wave Energy Resource Assessment and Characterization, International Electrotechnical Commission, Geneva, Switzerland, 2015, 2015.

[51] V. Ramos, J.V. Ringwood, Exploring the utility and effectiveness of the IEC (International Electrotechnical Commission) wave energy resource assessment and characterisation standard: a case study, Energy 107 (2016) 668–682, https://doi.org/10.1016/J.ENERGY.2016.04.053.

[52] K. Amarouche, A. Akpınar, M.B. Soran, S. Myslenkov, A.G. Majidi, M. Kankal, V. Arkhipkin, Spatial calibration of an unstructured SWAN model forced with CFSR and ERA5 winds for the Black and Azov Seas, Appl. Ocean Res. 117 (2021) 102962, https://doi.org/10.1016/J.APOR.2021.102962.

[53] H. Hersbach, B. Bell, P. Berrisford, S. Hirahara, A. Horányi, J. Muñoz-Sabater, J. Nicolas, C. Peubey, R. Radu, D. Schepers, A. Simmons, C. Soci, S. Abdalla, X. Abellan, G. Balsamo, P. Bechtold, G. Biavati, J. Bidlot, M. Bonavita, G. De Chiara, P. Dahlgren, D. Dee, M. Diamantakis, R. Dragani, J. Flemming, R. Forbes, M. Fuentes, A. Geer, L. Haimberger, S. Healy, R.J. Hogan, E. Hólm, M. Janisková, S. Keeley, P. Laloyaux, P. Lopez, C. Lupu, G. Radnoti, P. de Rosnay, I. Rozum, F. Vamborg, S. Villaume, J.N. Thépaut, The ERA5 global reanalysis, Q. J. R. Meteorol. Soc. 146 (2020) 1999–2049, https://doi.org/10.1002/QJ.3803.

[54] D.C. Kapoor, General bathymetric chart of the oceans (GEBCO), Mar. Geodesy 5 (1) (1981) 73–80.

[55] J.J. Westerink, C.A. Blain, R.A. Luettich, N.W. Scheffner, ADCIRC: an advanced threedimensional circulation model for shelves. Coasts and Estuaries, Report 2-User's Manual for ADCIRC-2DDI, US Army Corps of Engineers, Washington, DC, 1992.

[56] M. Zijlema, Computation of wind-wave spectra in coastal waters with SWAN on unstructured grids, Coast. Eng. 57 (2010) 267–277, https://doi.org/10.1016/j.coastaleng.2009.10.011.

[57] M.A. Hoque, W. Perrie, S.M. Solomon, Application of SWAN model for storm generated wave simulation in the Canadian Beaufort Sea, J. Ocean Eng. Sci. 5 (2020) 19–34, https://doi.org/10.1016/j.joes.2019.07.003.

[58] A. Mazzolari, Two-dimensional unstructured mesh generation applied to shallow water models. Doutoramento Em Engenharia Civil, Instituto Superior Técnico, 2013. PhD Thesis.

[59] A.G. Majidi, V. Ramos, P. Rosa Santos, L. das Neves, F. Taveira-Pinto, The impact of the SWAN model calibration on the energy production of wave energy converter systems. https://www.iahr.org/library/infor?pid=22196, 2022. (Accessed 26 April 2024).

[60] N. Guillou, G. Chapalain, Annual and seasonal variabilities in the performances of wave energy converters, Energy 165 (2018) 812–823, https://doi.org/10.1016/J.ENERGY.2018.10.001.

[61] L. Rusu, F. Onea, Assessment of the performances of various wave energy converters along the European continental coasts, Energy 82 (2015) 889–904, https://doi.org/10.1016/J.ENERGY.2015.01.099.

[62] A.G. Majidi, B. Bingölbali, A. Akpınar, G. Iglesias, H. Jafali, Downscaling wave energy converters for optimum performance in low-energy seas, Renew. Energy 168 (2021) 705–722, https://doi.org/10.1016/J.RENENE.2020.12.092.

[63] A.G. Majidi, B. Bingölbali, A. Akpınar, E. Rusu, Wave power performance of wave energy converters at high-energy areas of a semi-enclosed sea, Energy 220 (2021) 119705, https://doi.org/10.1016/J.ENERGY.2020.119705.

[64] A.G. Majidi, B. Bingölbali, A. Akpınar, Power production performance of different wave energy converters in the southwestern black sea, Int. J. Energy Power Eng. 14 (2020) 191–195.
[65] E. Rusu, Assessment of the wave energy conversion patterns in various coastal environments, in: Proceedings of 1st International E-Conference on Energies, MDPI, Sciforum.net, 2014, p. c015, https://doi.org/10.3390/ece-1-c015.
[66] L.D. Mann, Application of ocean observations & analysis: the CETO wave energy project, in: A. Schiller, G.B. Brassington (Eds.), Operational Oceanography in the 21st Century, Springer Netherlands, Dordrecht, 2011, pp. 721–729, https://doi.org/10.1007/978-94-007-0332-2_27.
[67] T. Shimura, N. Mori, H. Mase, Ocean waves and teleconnection patterns in the northern hemisphere. https://doi.org/10.1175/JCLI-D-12-00397.1, 2013.
[68] J.W. Hurrell, Y. Kushnir, M. Visbeck, The North atlantic oscillation, Science 291 (2001) 603–605, https://doi.org/10.1126/science.1058761.
[69] M.J. Rodwell, D.P. Rowell, C.K. Folland, Oceanic forcing of the wintertime North Atlantic oscillation and European climate, Nature 398 (1999) 320–323, https://doi.org/10.1038/18648.
[70] A. Semedo, The North Atlantic Oscillation Influence on the Wave Regime in Portugal: an Extreme Wave Event Analysis, 2005, p. 106.
[71] C. Izaguirre, F.J. Mendez, M. Menendez, A. Luceño, I.J. Losada, Extreme wave climate variability in southern Europe using satellite data, J. Geophys. Res.: Oceans 115 (2010), https://doi.org/10.1029/2009JC005802.
[72] J.W. Hurrell, H. Van Loon, Decadal variations in climate associated with the North atlantic oscillation, Climatic Change 36 (3) (1997) 301–326, https://doi.org/10.1023/A:1005314315270.
[73] L. Comas-Bru, F. McDermott, M. Werner, The effect of the East Atlantic pattern on the precipitation δ18O-NAO relationship in Europe, Clim. Dynam. 47 (2016) 2059–2069, https://doi.org/10.1007/s00382-015-2950-1.
[74] Climate Prediction Center - Teleconnections: North Atlantic Oscillation, (n.d.). https://www.cpc.ncep.noaa.gov/products/precip/CWlink/pna/nao.shtml (accessed December 21, 2024).
[75] Climate Prediction Center - East Atlantic (EA), (n.d.). https://www.cpc.ncep.noaa.gov/data/teledoc/ea.shtml (accessed December 21, 2024).
[76] J. Garrote, A. Díaz-Álvarez, H.V. Nganhane, G. Garzón Heydt, The severe 2013–14 winter storms in the historical evolution of cantabrian (northern Spain) beach-dune systems, Geosciences 8 (2018) 459, https://doi.org/10.3390/geosciences8120459.
[77] G. Masselink, B. Castelle, T. Scott, G. Dodet, S. Suanez, D. Jackson, F. Floc'h, Extreme wave activity during 2013/2014 winter and morphological impacts along the Atlantic coast of Europe, Geophys. Res. Lett. 43 (2016) 2135–2143, https://doi.org/10.1002/2015GL067492.
[78] A. Ulazia, M. Penalba, A. Rabanal, G. Ibarra-Berastegi, J. Ringwood, J. Sáenz, Historical evolution of the wave resource and energy production off the Chilean coast over the 20th century, Energies 11 (2018) (2018) 2289, https://doi.org/10.3390/EN11092289. Vol. 11, Page 2289.
[79] L. Castro-Santos, D. Silva, A.R. Bento, N. Salvação, C.G. Soares, Economic feasibility of wave energy farms in Portugal, Energies 11 (2018) (2018) 3149, https://doi.org/10.3390/EN11113149. Vol. 11, Page 3149.
[80] S. Bozzi, G. Besio, G. Passoni, Wave power technologies for the Mediterranean offshore: scaling and performance analysis, Coast. Eng. 136 (2018) 130–146, https://doi.org/10.1016/j.coastaleng.2018.03.001.
[81] G. Reikard, B. Robertson, J. Bidlot, Combining wave energy with wind and solar: short-term forecasting, Renew. Energy 81 (2015) 442–456, https://doi.org/10.1016/j.renene.2015.03.032.
[82] J. Morim, N. Cartwright, M. Hemer, A. Etemad-Shahidi, D. Strauss, Inter- and intra-annual variability of potential power production from wave energy converters, Energy 169 (2019) 1224–1241, https://doi.org/10.1016/J.ENERGY.2018.12.080.
[83] A. Babarit, J. Hals, M.J. Muliawan, A. Kurniawan, T. Moan, J. Krokstad, Numerical benchmarking study of a selection of wave energy converters, Renew. Energy 41 (2012) 44–63, https://doi.org/10.1016/j.renene.2011.10.002.
[84] A. Gul Majidi, B. Bingölbali, A. Akplnar, E. Rusu, Dimensionless normalized wave power in the hot-spot areas of the black sea, E3S Web of Conferences 173 (2020), https://doi.org/10.1051/E3SCONF/202017301001.
[85] N. Almonacid, Evaluating a Project for Wave Energy Generation at a Coastal Site in Chile, University of Southampton, Faculty of Engineering and Environment, 2015. Master's thesis.
[86] J.C. Pacaldo, P.H.T. Bilgera, M.L.S. Abundo, Nearshore wave energy resource assessment for off-grid islands: a case study in cuyo island, palawan, Philippines, Energies 15 (2022) 8637, https://doi.org/10.3390/en15228637.
[87] X. Shi, S. Li, B. Liang, J. Zhao, Y. Liu, Z. Wang, Numerical study on the impact of wave-current interaction on wave energy resource assessments in Zhoushan sea area, China, Renew. Energy 215 (2023) 119017, https://doi.org/10.1016/j.renene.2023.119017.
[88] S. Derakhshan, M. Moghimi, H. Motawej, Development of a Mathematical Model to Design an Offshore Wind and Wave Hybrid Energy System, vol. 6, 2018.
[89] G. Giannini, P. Rosa-Santos, V. Ramos, F. Taveira-Pinto, Wave energy converters design combining hydrodynamic performance and structural assessment, Energy 249 (2022) 123641, https://doi.org/10.1016/j.energy.2022.123641.
[90] D. Silva, E. Rusu, C.G. Soares, Evaluation of various technologies for wave energy conversion in the Portuguese nearshore, Energies 6 (2013) (2013) 1344–1364, https://doi.org/10.3390/EN6031344, 1344-1364 6.